國立交通大學

光電工程研究所

碩士論文

K·P 理論於玻色–愛因斯坦凝聚態在光晶格之應用

The K·P theory in Bose-Einstein condensates in optical lattices

研究生：陳映如

指導教授：謝文峰 教授

中華民國九十三年六月

K·P 理論於玻色-愛因斯坦凝聚態在光晶格之應用

The K·P theory in Bose-Einstein condensates in optical lattices

研 究 生：陳映如　　Student: Ying-Ru Chen

指導教授：謝文峰　　Advisor: Wen-Feng Hsieh

國 立 交 通 大 學

光電工程研究所

碩 士 論 文

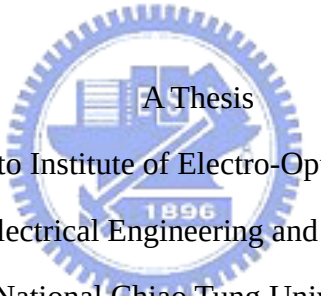

A Thesis

Submitted to Institute of Electro-Optical Engineering

College of Electrical Engineering and Computer Science

National Chiao Tung University

in partial Fulfillment of the Requirements

for the Degree of

Master

in

Electro-Optical Engineering

June 2004

Hsinchu, Taiwan, Republic of China

中華民國九十三年六月

K·P理論於玻色-愛因斯坦凝聚態在光晶格之應用

研究生：陳映如　　指導老師：謝文峰 教授

國立交通大學光電工程研究所

摘要

我們利用K·P(等效質量)理論探討具有吸引力或排斥力的玻色-愛因斯坦凝聚態在光晶格之特性。 玻色-愛因斯坦凝聚態的波函數可由 Gross-Pitaevskii 方程式描述。 當玻色-愛因斯坦凝聚態的能量接近能帶邊界(band edge)時，其波函數就可藉由等效質量理論得到解析解，即布拉格函數乘上由等效質量方程式得到之波包函數。 利用這樣的波函數，我們探討亮孤子及暗孤子在能帶結構中所表現之特性，並依其波函數之特性分類為布拉格反射型及全反射型的孤子。在推導等效質量方程式過程中，我們保留能帶(band edge energy)這一項，並驗證此項對於描述玻色-愛因斯坦凝聚態在光晶格有重要意義。 此外，我們利用數值解 Gross-Pitaevskii 方程式來驗證由等效質量理論推得的解析解之準確性，並與 Eiermann 等人的實驗結果做比較。 我們證實玻色-愛因斯坦凝聚態在光晶格之特性不但可以 ”定性” 更可 ”定量” 地運用等效質量理論來描述。

The $K \cdot P$ theory in Bose-Einstein condensates in optical lattices

Student: Ying-Ru Chen Advisor: Prof. Wen-Feng Hsieh

Institute of Electro-optical Engineering
National Chaio Tung University

Abstract

We apply the $K \cdot P$ (effective mass) theory to study the dynamics of Bose-Einstein condensates (BECs) in optical lattices with either attractive or repulsive atom interactions. The macroscopic condensate wave function is described by Gross-Pitaevskii (G-P) equation. Near band edge, we obtain the analytic condensate wave function which is deduced from the effective mass theory and is found to be a Bloch function modulated by a soliton envelope function of the effective mass equation. We demonstrate that bright and dark solitons, corresponding to energy in band gap and energy within band, respectively, can exist for both attractive and repulsive atom interactions and can be categorized as Bragg reflection and internal reflection type solitons. In deriving the effective mass equation, we preserve the band edge energy term and we show this term is important to describe BECs in optical lattices. Numerically solving the G-P equation confirms the analytic results that agree reasonably well with simulations as well as compared with the experimental results reported by Eiermann *et al.* We demonstrate that BECs in optical lattices can be described, qualitatively and quantitatively, by the effective-mass theory.

誌　　謝

兩年的交大研究生生涯即將劃下句點。　首先，我必須感謝我的指導老師謝文峰教授以其淵博學問教導我的課業及研究，提供一個好的研究環境讓我自由發揮，並在當我遇到研究困難時，仔細地、耐心地和我討論，引導出新的方向前進。我也要感謝文化大學物理系程思誠教授，在我的研究過程中給予豐富的專業知識，提供完整的理論架構及新的想法讓我努力實行，也因而不斷地學習、進步。

感謝實驗室的夥伴們在這兩年和我一起成長，我的研究生活因你們而添增不少樂趣！　實驗室的大家長家弘、阿政、小戴、智章學長及美麗晴如學姐；帶領我進入光晶領域的智賢、阿倫學長；我親愛的同學們:患難與共的小白同學、自以為帥的阿猴、”鬆”師傅、光子晶體組團對夥伴: 和良、育儒、珮芳及秉洲；貼心可愛的學弟妹: 聒聒俊毅、溫柔阿笑、耍寶國峰、小豪，以及我們光晶組一脈單傳的家斌(加油喔~)。　還有，還有感謝那垂了一隻耳該減肥的奶油學長不分晝夜的陪伴!

此外，更感謝我的家人爸、媽、姐姐和弟弟對我的支持與關心!

最後，感謝國科會(計畫編號 NSC 92-2112-M009-037)的經費支持，使得本研究得以順利完成。

于 風城交大 民國九十三年六月

Content

List of Figures

Chapter 1 Introduction

1-1 Preface

Bose-Einstein condensates were predicted in 1924 by S. N. Bose and A. Einstein. S. N. Bose, an Indian physicist, worked out the statistics for photons. A. Einstein applied Bose's statistical model to predict that almost all of the particles in a Bosonic system would congregate in the ground state at an ultra-low temperature. Particles, in this case, are referred to atoms or molecules. They are bosonic (fermionic) if they have integer (half-integer) spin, or equivalently, if the total number of electrons, protons, and neutrons they contain is even (odd). For fermions, the Pauli exclusion principle prevents two particles from occupying the same quantum state, whereas, for bosons, the probability of finding particles in the same quantum state increases dramatically and satisfy the distribution of Bose-Einstein statistics given by

$$N(E) = \frac{1}{e^{(E-\mu)/k_B T} - 1}$$

where k_B is Boltzmann's constant, μ is the chemical potential, T is temperature and E is the energy of particles. As a gas of bosonic particles is cooled to below a critical temperature and are all in ground state, De Broglie's matter waves are comparable to the distance between particles, the individual wavepackets start to overlap and then these waves start to oscillate in coherent. These bosonic particles are called Bose-Einstein condensates (BECs). Since all atoms of BECs occupy the same ground state energy, the many-body wave function is then the product of N identical single-particle where N is the number of condensate atoms. This single-particle wave function is therefore called the condensate wave function or

macroscopic wave function. If the number of atoms is high, BECs exhibit cubic nonlinearity which is equivalent to Kerr nonlinearity in optics due to interatomic forces of condensate atoms, characterized by the s-wave scattering length a_s (typically 1 to 5 nm for alkali atoms). In a gas, the separation between atoms $n^{-1/3}$ is much larger than the effective range of the interatomic forces, i.e. the quantity $na_s^3 \ll 1$. This inequality expresses that binary collisions are much more frequent than three-body collisions. It is in this limit that the theory of the weakly interacting Bose gas applies. Under weak atomic interaction condition, condensate wave functions of BECs in optical lattices can be described by the Gross-Pitaevskii (G-P) equation, or equivalently, the nonlinear Schrödinger equation with periodic potentials.

BECs could not be observed until cooling techniques were developed to reach such a low temperature, because creation of BECs accompany with ultra-low temperature (around billionths of a degree above absolute zero). S. Chu, C. Cohen-Tannoudji and W.D. Phillips who won the Nobel Prize in Physics in 1997 developed methods to cool and trap atoms with laser light. This achievement accomplishes the first observation of BEC in dilute alkali gas in 1995 by E.A. Cornell, W. Ketterle and C.E. Wieman who won the Nobel Prize in Physics in 2001. With successful experimental observation of BECs, many physical properties of BECs can be investigated further such as loading BECs in optical lattices [1] generated by interference of laser beams. The first experiments involving the dynamics of BECs in periodic potentials were carried out by Anderson and Kasevich, who used this approach to demonstrate a mode-locked atom laser [2], and observe atomic Josephson oscillations [2,3]. In addition, the properties of coherent macroscopic matter waves in a lattice, such as the Bloch-band structure [4], macroscopic interference effects [2],

Bloch oscillations and Landau–Zener tunnelling [5], have been explored in a number of experiments.

Due to the potential wells being separated by a finite distance, atoms can tunnel between adjacent wells. BECs in optical lattices are affected by the structures of optical lattices. The BEC spectrum has a band-gap structure [6], no BEC states can exist within the band gap in a linear regime, where the number of atoms is low. If the number of atoms is high, BECs behave nonlinearly. As the nonlinear term in the wave equation exactly compensates for wavepacket dispersion, solitons occur. There are spatially localized nonlinear BEC states, called gap, or equivalently bright, solitons which exist within the band gaps [7]. As the energy is in band, there exist dips on condensate density and a sharp phase gradient of the wave function at the position of the minimum and are called dark solitons. Without optical lattices, bright solitons of BECs can only exist with attractive nonlinearity ($a_s < 0$) below a certain number of atoms [8]. On the contrary, dark solitons can only exist under repulsive nonlinearity ($a_s > 0$). However, bright and dark matter wave solitons is stable under both attractive and repulsive nonlinearity and have no restriction of number of atoms in BECs due to the periodicity of the optical lattice which leads to the effective dispersion of the BEC wavepakets deduced from the band structure.

1-2 Motivation

Since the governing equation of BECs in optical lattices, G-P equation, is nonintegrable, several different theories whose accuracy depends heavily on the nature of the underlying problem are used to find the approximated solutions. The

tight binding approximation [9] is only accurate when the potentials are deep and well separated. The coupled-mode theory is valid when the energies are close to the gap and shallow potentials. An accurate solution of solitons can only be obtained by exactly solving the full nonlinear Schrödinger equation with a periodic potential. Louis *et al.* [10] analyzed numerically the existence and stability of spatially extended and localized states of BEC loaded into an optical lattice. They demonstrated the existence of families of spatially localized matter-wave solitons existing at gaps. Efremidis *et al.* [11] studied numerically the properties of gap solitons in BECs with either attractive or repulsive atom interaction. They found families of gap solitons, which are characterized by the position of the energy eigenvalue within the associated band structure. However, numerical simulations of BECs in optical lattices are highly computationally intensive, we describe Bose-Einstein condensates in one-dimensional optical lattices by introducing the effective-mass theory which has been extended to study semiconductor superlattices successfully without the need for full-scale numerical calculations. Pu *et al.* [12] have obtained an effective equation of motion governing the time evolution of the envelope of the condensate wave function in which the periodic external potential appears in the form of an effective mass. Numerical calculation confirmed that this envelope function approach provides us with useful qualitative insight into the condensate dynamics.

In the Thesis, we study the nonlinear effect of BECs in one-dimensional optical lattices, numerically and analytically. With a little modification, we add a term, band energy at a specific wave-vector, to the effective mass equation [12] of the envelope wave function of BECs in which the periodic external potential appears in the form of an effective mass. Accordingly, we obtain analytical solution of the wave function

of soliton solution which is a Bloch function from periodicity times the envelope function of the nonlinear effective-mass Schrödinger equation. We will theoretically observe the appearance of bright and dark solitons correspond to energy in and out-of band gap under different sign of the s-wave scattering length a_s. The analytic solutions of BECs are compared with the numerical results of the G-P equation. We find that BECs in optical lattices can be described, qualitatively and quantitatively, by the effective-mass theory.

1-3 Organization of the Thesis

This Thesis is organized as follows. Chapter 2 gives a brief review of effective mass theory and a deduction of the effective mass of BECs in optical lattices. The plane wave method is applied to study the linear regime of BECs in optical lattices to obtain the band structure. In Chapter 3, the one-band effective mass theory of a G-P equation is introduced which gives analytic bright/dark soliton solution. We give the comparisons between analytic and numerical results. Comparisons between analytic and experimental results reported by Eiermann *et al.* are also included. We give a brief conclusion in Chapter 4.

Chapter 2 Theory and Methodology

The dynamics of Bose-Einstein condensates (BECs) can be approximately described in the mean-field approximation by the Gross-Pitaevskii (G-P), or nonlinear Schrödinger, equation for the macroscopic condensate wave function. BECs in optical lattices have many special phenomena, which are created by the interference between the nonlinearity due to the atomic interactions and the exotic dispersion relations from the periodic potential produced by interference of laser beams. The chemical potential of atoms trapped in a period potential exhibits band structures containing band gaps. No linear eigenmodes exist within a band gap. Louis *et al.*[10] demonstrated numerically that there are nonlinear localized modes of the condensate existing in the band gap, which are matter-wave gap solitons. On the other hand, dispersion relations of photons in nonlinear photonic crystal also exhibit the band-gap structure. Nonlinear localized photon-modes, which are optical gap solitons [13], are shown inside the photonic gap [14, 15].

To understand the physical properties of the gap soliton, the one-band effective-mass theory of a nonlinear Schrödinger equation is derived and solved analytically to obtain gap soliton solutions. We start with G-P equation to describe the dynamics of BECs in optical lattices. The linear band structure of BECs in optical lattices is solved by the coupled mode theory. The effective mass of BECs is defined. The numerical simulation method is also given.

2-1 Bose-Einstein condensates in optical lattices

The dynamics of a Bose-Einstein condensate in an optical lattice can be described by the Gross-Pitaevskii (GP) [16] or the nonlinear Schrödinger equation for

the macroscopic condensate wave function $\Psi(\mathbf{r},t)$,

$$i\hbar\frac{\partial\Psi(\mathbf{r},t)}{\partial t}=\left[\frac{-\hbar^2}{2m}\nabla^2+V(x)+U(\mathbf{r})+g|\psi|^2\right]\Psi(\mathbf{r},t), \tag{2.1}$$

where $\hbar$ is Planck's constant, m is the mass of the atoms, $g=4\pi a_s\hbar^2/m$ is the nonlinear coefficient, and a_s is the *s*-wave scattering length. $V(x)=E_o\sin^2(\pi x/L)$ is a one-dimensional periodic potential produced by the interference of laser beams, where L is the lattice constant and E_o is the potential depth. $U(\mathbf{r})=\frac{1}{2}m\left[\omega_x^2x^2+\omega_\perp^2(y^2+z^2)\right]$ is an optical trapping potential with frequencies ω_x and $\omega_\perp$. Due to the high confinement in the *y*-*z* plane, the trap is elongated along the *x* direction (i.e. $\omega_x\ll\omega_\perp$). Therefore, we express the wave function as $\Psi(\mathbf{r};t)=a(y,z)\psi(x,t)$, where $a(y,z)$ is described by a solution of the two-dimensional radially symmetric quantum harmonic-oscillator problem, $(-\hbar^2/2m)\nabla_\perp^2a+(m\omega_\perp^2/2)(x^2+y^2)a=\hbar\Omega_\perp a$. By applying the transformation $\psi\to\psi\exp(-i\Omega_\perp t)$ and integrating Eq. (2.1) in the *y*-*z*, a one-dimensional G-P equation is derived as

$$i\hbar\frac{\partial\psi(x,t)}{\partial t}=\left[\frac{-\hbar^2}{2m}\frac{\partial^2}{\partial x^2}+E_o\sin^2(\frac{\pi}{L}x)+\frac{g}{2}|\psi|^2\right]\psi(x,t). \tag{2.2}$$

It is more convenient to use dimensionless quantities by normalizing $T=t/T_o$, $X=x/(L/2)$, $\psi=\varphi/L_1^{1/2}$, and $V_o=E_o/E_r$, and choose $T_o=mL^2/4\hbar$, $L_1=\omega_\perp|a_s|mL^2/2\hbar$, and $E_r=4\hbar^2/mL^2$. After these transformations, an effective one-dimensional G-P equation in dimensionless variables is derived as

$$i\hbar\frac{\partial\varphi(X,T)}{\partial T}=\left[\frac{-1}{2}\frac{\partial^2}{\partial X^2}+V_o\sin^2\left(\frac{\pi}{2}X\right)+\sigma|\varphi|^2\right]\varphi(X,T), \tag{2.3}$$

where $\sigma=sgn(a_s)$. Eq.(2.3) is equivalent to a time-dependent nonlinear

Schrödinger equation with a periodic potential. If σ is positive (negative), atoms are resulting in repulsive (attractive) interaction. Eq.(2.3) possesses an integral of motion

$$N = \int_{-\infty}^{\infty} |\varphi|^2 \, dX \,, \tag{2.4}$$

which accounts for the conservation of the number N of atoms in the condensate.

2-1-1 Band Structure

The E-k band structure of a BEC in optical lattices determines basic properties of the matter waves under linear Schrödinger equation. To find the band structure we assume that the linear part of Eq. (2.3) admits stationary solutions of the form $\varphi(X,T) = \phi(X)\exp(-iET)$, thus obtaining the following eigenvalue problem,

$$E\ \phi(X) = \left[\frac{-1}{2}\frac{\partial^2}{\partial X^2} + V_o \sin^2\left(\frac{\pi X}{2}\right)\right]\phi(X). \tag{2.5}$$

Eq. (2.5) possesses periodic solutions, known as Floquet-Bloch (FB) modes. By using plane-wave methods, the periodic potential $V_o \sin^2(\pi X/2)$ can be expanded as

$$\frac{V_o}{2} - \frac{V_o\left(e^{i\pi X} + e^{-i\pi X}\right)}{4}.$$

The Bloch functions can be expressed as

$$\phi(X,k) = \sum_m a_m e^{i(k+m\pi)X} \,, \tag{2.6}$$

and satisfy orthonormality

$$\int_{cell} \phi_l^*(X,q)\phi_m(X,k)dx = \delta_{lm}\delta(k-q). \tag{2.7}$$

Substituting Eq.(2.6) into Eq.(2.5), we have

$$\left(2E - V_o - \left(k + m\pi\right)^2\right)a_m + \frac{V_o}{2}a_{m-1} + \frac{V_o}{2}a_{m+1} = 0\,. \tag{2.8}$$

The accuracy of the method depends on the number of plane waves considered in the expansion, as well as on the form and the depth of the potential. We assume the potential is relatively shallow, and the Bloch modes between the first and the second band can be accurately described by keeping only two terms of the expansion, i.e. $m = 0, -1$. Eq.(2.6) is rewritten as

$$\phi(X,k) = a_o e^{ikX} + a_{-1}e^{ikX}e^{-i\pi X}\,. \tag{2.9}$$

Considering the dominant terms in Eq.(2.8), we obtain the following coupled equations

$$\begin{cases} \left(2E - V_o - k^2\right)a_o + \dfrac{V_o}{2}a_{-1} = 0 \\ \dfrac{V_o}{2}a_o + \left(2E - V_o - \left(k - \pi\right)^2\right)a_{-1} = 0 \end{cases} \tag{2.10}$$

We substitute Eq.(2.9) into Eq.(2.7) to satisfy the orthonormality of the Bloch functions, and then the coefficients a_o and a_{-1} are given by

$$\left|a_o\right|^2 = \left|a_{-1}\right|^2 = \frac{1}{4\pi} \tag{2.11}$$

Substituting these coefficients into the Bloch functions in Eq.(2.9), we obtain the lower band Bloch waves at wave vector k

$$\phi(X,k) = e^{ikX}\frac{1}{\sqrt{4\pi}}\left(1 + e^{-i\pi X}\right) \tag{2.12}$$

And, the upper band Bloch waves at wave vector k

$$\phi(X,k) = e^{ikX}\frac{i}{\sqrt{4\pi}}\left(-1 + e^{-i\pi X}\right) \tag{2.13}$$

We have a nontrivial solution in Eq.(2.10), when the determinant of coefficients vanishes. *E-k* band structure of BECs in one-dimensional optical lattices is then derived as

$$E = \frac{V_o}{2} + \frac{k^2 + (k-\pi)^2}{4} \pm \frac{\sqrt{(k^2 - (k-\pi)^2)^2 + {V_o}^2}}{4} \tag{2.14}$$

The wave-vector k lies in the first Brillouin zone which is $-\pi/2 \le k \le \pi/2$. For $V_o = 2.5$, the band structure is as in Fig. 1. We first consider the two lowest bands at the extreme point of the first Brillouin zone i.e. $k = \pi/2$. E_a, the lower energy band at $k = \pi/2$, is given by

$$E_a = \frac{\pi^2}{8} + \frac{1}{4}V_o \tag{2.15}$$

And, E_b, the upper energy at $k = \pi/2$, is given by

$$E_b = \frac{\pi^2}{8} + \frac{3}{4}V_o \tag{2.16}$$

We therefore obtain the second band gap $\Delta E = V_o / 2$ at $k = \pi / 2$. Finally, we can derive the Bloch waves at energy bands at $k = \pi/2$ from Eq.(2.12) and Eq.(2.13). At the energy, E_a, the Bloch wave is an even function given by

$$\phi_a(X, \frac{\pi}{2}) = \frac{1}{\sqrt{4\pi}} 2\cos\left(\frac{\pi}{2}X\right) \tag{2.17}$$

And at the energy, E_b, the Bloch wave is an odd function given by

$$\phi_b(X, \frac{\pi}{2}) = \frac{1}{\sqrt{4\pi}} 2\sin\left(\frac{\pi}{2}X\right) \tag{2.18}$$

The condensate wave function in the lowest energy of the first band at k=0 is given by

$$\phi_c(X, 0) = \left(b_o + b_{-1}\cos\pi X\right) \tag{2.19}$$

We solved Eq.(2.7) to obtain b_o and b_{-1}, which are given by

$$\begin{pmatrix} b_o \\ b_1 \end{pmatrix} = \frac{1}{\sqrt{2\pi}\sqrt{\pi^4 + 2{V_o}^2} - \pi^2\sqrt{\pi^4 + 2{V_o}^2}} \begin{pmatrix} V_o \\ \sqrt{\pi^4 + 2{V_o}^2} - \pi^2 \end{pmatrix} \tag{2.20}$$

E_c, the energy at $k = 0$, is given by

$$E_c = \frac{V_o}{2} + \frac{\pi^2}{4} - \frac{\sqrt{\pi^4 + 2V_o^2}}{4} \tag{2.21}$$

The first band gap is explicitly $\Delta E = E_c$ since E_c is the lowest energy in the *E-K* spectrum.

Up to the present, we have derived the energy band structure and obtained three Bloch functions, named $\phi_a(X)$, $\phi_b(X)$ and $\phi_c(X)$ at chosen points in the *E-K* structure under the linear regime of the nonlinear Schrödinger equation with periodic potentials.

In the following, we will introduce the effective-mass theory to the nonlinear Schrödinger equation with periodic potentials. The envelop wave function of BECs in a periodic potential can be described by an effective nonlinear Schrödinger equation, where the periodicity is absorbed into the effective mass.

2-2 The Effective Mass Theory

Effective mass theory is a well-known approximation in solid state physics for studying dynamics of an electron in semiconductor, described by nonlinear Schrödinger equation. The dynamics of a Bose-Einstein condensate loaded into an optical lattice are described by the Gross-Pitaevskii (G-P) equation. The two systems, electrons in semiconductor and BECs in optical lattices, are analogous. Therefore, we can introduce the effective mass theory to study BECs in optical lattices.

2-2-1 Brief review of effective mass theory

We give a brief review of effective mass theory in solid state system [17]. Starting with a general form of *linear* Schrödinger equation

$$\left(H_o + U\right)\varphi\left(\mathbf{r},t\right) = i\hbar\frac{\partial\varphi\left(\mathbf{r},t\right)}{\partial t} \tag{2.22}$$

where H_o is a time independent Hamiltonian that, in most instance, contains a periodic potential. U represents an external influence; it is not periodic and may be time dependent. The eigenfunctions of the characteristic equation given by

$$H_o\phi_n\left(\mathbf{k},\mathbf{r}\right) = E_n\phi_n\left(\mathbf{k},\mathbf{r}\right) \tag{2.23}$$

are the Bloch functions with $\phi_n(\mathbf{k},\mathbf{r}) = \phi_n(\mathbf{k},\mathbf{r}+\mathbf{a})$. Here $\mathbf{k}$ is the wave vector, n is the band index and $\mathbf{a}$ is the lattice vector. The Bloch functions are orthonormal according to

$$\int\phi_n^*\left(\mathbf{q},\mathbf{r}\right)\,\phi_l\left(\mathbf{k},\mathbf{r}\right)d^3r = \delta_{nl}\delta\left(\mathbf{k}-\mathbf{q}\right). \tag{2.24}$$

Note that in this equation and everywhere else, the integral on **r** involves complete space. They also form a complete set that

$$\sum_n\int\phi_n^*\left(\mathbf{k},\mathbf{r}\right)\,\phi_l\left(\mathbf{k},\mathbf{r}'\right)d^3k = \delta\left(\mathbf{r}-\mathbf{r}'\right). \tag{2.25}$$

It is sometimes desirable to expand the wave function simply related to the Bloch functions at a single **k**-point of a band structure. Therefore, we introduce a basis of the so-called Kohn-Luttinger functions $\chi_n\left(\mathbf{k},\mathbf{r}\right)$ which are defined in terms of the Bloch functions at some conveniently chosen point in the first Brillouin zone $\mathbf{k_0}$ as

$$\chi_n\left(\mathbf{k},\mathbf{r}\right) = e^{i(\mathbf{k}-\mathbf{k}_0)\cdot\mathbf{r}}\phi_n\left(\mathbf{k_0},\mathbf{r}\right) = e^{i\mathbf{k}\cdot\mathbf{r}}u_n\left(\mathbf{k_0},\mathbf{r}\right), \tag{2.26}$$

where u_n is the cell periodic function. The Kohn-Luttinger functions obey the same orthonormality and completeness relations as the Bloch functions. Thus, an arbitrary wave function can be expanded as

$$\varphi(\mathbf{r},t) = \sum_n\int A_n\left(\mathbf{k},t\right)\chi_n\left(\mathbf{k},\mathbf{r}\right)d^3k\,, \tag{2.27}$$

where $A_n\left(\mathbf{k},t\right)$ are the expansion coefficients. And the matrix elements of H_o are determined as the follows

$$\begin{aligned}\left[n\mathbf{k}\left|H_o\right|l\mathbf{q}\right] &= \int \chi_n^*(\mathbf{k},\mathbf{r})\, H_o \chi_l(\mathbf{q},\mathbf{r})\, d^3r \\ &= \int e^{i(\mathbf{q}-\mathbf{k})\cdot\mathbf{r}} u_n^*(\mathbf{k_o},\mathbf{r}) \\ &\quad \times\left[E_l(\mathbf{k_o}) + (\hbar/m)(\mathbf{q}-\mathbf{k_o})\cdot\mathbf{p} + \left(\hbar^2/2m\right)\left(\mathbf{q}^2-\mathbf{k_o}^2\right)\right] \\ &\quad \times u_l(\mathbf{k_o},\mathbf{r})\, d^3r\end{aligned} \tag{2.28}$$

We can break up the integral over whole space into an integral over unit cells since $\mathbf{p}u_l(\mathbf{k_o},\mathbf{r})$ is periodic if u_l is periodic.

$$\int e^{i(\mathbf{q}-\mathbf{k})\cdot\mathbf{r}}\; u_n^*(\mathbf{k_o},\mathbf{r})\;\mathbf{p}\;u_l(\mathbf{k_o},\mathbf{r})\; d^3r = \delta(\mathbf{q}-\mathbf{k})\mathbf{p}_{nl}(\mathbf{k_o}) \tag{2.29}$$

where

$$\mathbf{p}_{nl}(\mathbf{k_o}) = \frac{(2\pi)^3}{\Omega}\int_{cell} u_n^*(\mathbf{k_o},\mathbf{r})\mathbf{p}u_l(\mathbf{k_o},\mathbf{r})\, d^3r \tag{2.30}$$

with Ω being the volume of a unit cell. Thus, Eq.(2.28) yields

$$\begin{aligned}&\left[n\mathbf{k}\left|H_o\right|l\mathbf{q}\right] \\ &= \delta(\mathbf{q}-\mathbf{k})\left\{\delta_{nl}\left[E_l + \left(\hbar^2/2m\right)\left(\mathbf{q}^2-\mathbf{k_o}^2\right)\right] + (\hbar/m)(\mathbf{q}-\mathbf{k_o})\cdot\mathbf{p}_{nl}(\mathbf{k_o})\right\}\end{aligned} \tag{2.31}$$

Consequently, the expansion coefficients $A_n(\mathbf{k},t)$ of Eq.(2.27) satisfy

$$\begin{aligned}&\left[E_n + \left(\hbar^2/2m\right)\left(\mathbf{q}^2-\mathbf{k_o}^2\right) - i\hbar\partial/\partial t\right] A_n(\mathbf{k},t) \\ &\quad + (\hbar/m)(\mathbf{q}-\mathbf{k_o})\cdot\sum_l \mathbf{p}_{nl}(\mathbf{k_o})\, A_l(\mathbf{k},t) \\ &\quad + \sum_l \int d^3q \left[n\mathbf{k}\left|U\right|l\mathbf{q}\right] A_l(\mathbf{q},t) = 0\end{aligned} \tag{2.32}$$

This is the Schrödinger equation under the effective mass theory. For a stationary state of energy E, i.e., $A_n(\mathbf{k},t) \to A_n(\mathbf{k})$, Eq.(2.32) can be represented as

$$\begin{aligned}&\left[E_n + \left(\hbar^2/2m\right)\left(\mathbf{q}^2-\mathbf{k_o}^2\right) - E\right] A_n(\mathbf{k}) \\ &\quad + (\hbar/m)(\mathbf{q}-\mathbf{k_o})\cdot\sum_l \mathbf{p}_{nl}(\mathbf{k_o})\, A_l(\mathbf{k}) \\ &\quad + \sum_l \int d^3q \left[n\mathbf{k}\left|U\right|l\mathbf{q}\right] A_l(\mathbf{q}) = 0\end{aligned} \tag{2.33}$$

After some algebra, the last term in Eq.(2.33) is represented as

$$\left[n\mathbf{k}\middle|U\middle|l\mathbf{q}\right]=\delta_{nl}U\left(\mathbf{k}-\mathbf{q}\right)=\delta_{nl}\frac{1}{\left(2\pi\right)^3}\int e^{i(\mathbf{k}-\mathbf{q})\cdot\mathbf{r}}U\left(\mathbf{r}\right)d^3r\,. \tag{2.34}$$

The only terms of Eq.(2.33), which represent coupling between bands, are those involving the momentum matrix elements $\mathbf{p}_{nl}$.

We will consider the simpler non-degenerate case in the following discussion. By introducing a unitary transformation $C=e^{-iS}A$ to the expansion coefficients, where S is Hermitian and is in some sense "small", Eq.(2.33) is then replaced by

$$\begin{aligned}&\left[E_n+\left(\hbar^2/2m\right)\left(\mathbf{q}^2\text{-}\mathbf{k_o}^2\right)+\sum_j\left(\hbar/m^2\,\omega_{nj}\right)\left(\delta\mathbf{k}\bullet\mathbf{p}_{nj}\right)\left(\delta\mathbf{k}\bullet\mathbf{p}_{jn}\right)\right]C_n\left(\mathbf{k}\right)\\&\quad-E\;C_n\left(\mathbf{k}\right)+\int d^3q\;U\left(\mathbf{k}-\mathbf{q}\right)\;C_n\left(\mathbf{q}\right)=0\end{aligned} \tag{2.35}$$

By using ordinary perturbation theory, the energy of a state in the nth band at $\mathbf{k}$ is related to that at $\mathbf{k_o}$ in the second order by

$$\begin{aligned}E_n\left(\mathbf{k}\right)=E_n\left(\mathbf{k_o}\right)+\frac{\hbar}{m}\delta\mathbf{k}\bullet\mathbf{p}_{nn}+\frac{\hbar^2}{2m}\left(\mathbf{k}^2-\mathbf{k}_o^2\right)\\+\frac{\hbar^2}{m^2}\sum_{j(j\neq l)}\frac{\left(\delta\mathbf{k}\bullet\mathbf{p}_{nj}\right)\left(\delta\mathbf{k}\bullet\mathbf{p}_{jn}\right)}{E_n\left(\mathbf{k_o}\right)-E_j\left(\mathbf{k_o}\right)}\end{aligned} \tag{2.36}$$

The first three terms in Eq.(2.35) are equivalent to the expression given in the Eq.(2.36) for the energy as a function of wave vector to second order in $\delta\mathbf{k}$, so that we replace those terms by $E_n\left(\mathbf{k}\right)$

$$\left(E_n\left(\mathbf{k}\right)-E\right)C_n\left(\mathbf{k}\right)+\int d^3q\;U\left(\mathbf{k}-\mathbf{q}\right)\;C_n\left(\mathbf{q}\right)=0 \tag{2.37}$$

This equation resembles the Schrödinger equation in momentum space for one particle in the potential U. There is a significant difference in that the effective mass tensor m^* is involved, rather than the free electron mass m_o. All of the effects of the periodic potential are incorporated in the effective mass.

It is desirable to transform Eq.(2.37) to a differential equation in ordinary space. We

define a function $F_n(\mathbf{r})$ by

$$F_n(\mathbf{r}) = \int e^{i\delta\mathbf{k}\cdot\mathbf{r}} C_n(\mathbf{k}) d^3k \tag{2.38}$$

The integration in Eq.(2.38) includes only the Brillouin zone. Next, multiply Eq.(2.37) by $\exp(i\delta\mathbf{k}\cdot\mathbf{r})$ and integrate over the Brillouin zone. Let us consider the term

$$\int E(\mathbf{k}) e^{i\delta\mathbf{k}\cdot\mathbf{r}} C_n(\mathbf{k}) d^3k \tag{2.39}$$

where $E(\mathbf{k})$ can be expressed as

$$E(\mathbf{k}) = E_n + \sum \alpha_{ij}\ \delta k_i\ \delta k_j \tag{2.40}$$

where α_{ij} is the reciprocal effective mass tensor, given implicitly in Eq.(2.35) for $\left(m/m_n^*\right)_{\alpha\beta} = \left(m/\hbar^2\right)\left(\partial^2 E_n/\partial k_\alpha \partial k_\beta\right)$. By substituting Eq.(2.35) into Eq.(2.38) we have

$$\begin{aligned} & E_n\ F_n(\mathbf{r}) + \sum \alpha_{ij} \int \delta k_i\ \delta k_j\ e^{i\delta\mathbf{k}\cdot\mathbf{r}}\ C_n(\mathbf{k}) d^3k \\ &= E_n\ F_n(\mathbf{r}) + \sum \alpha_{ij} \frac{\partial}{i\partial x_i} \frac{\partial}{i\partial x_j} F_n(\mathbf{r}) \\ &= E_n \frac{1}{i\nabla} F_n(\mathbf{r}) \end{aligned} \tag{2.41}$$

The expression $E_n(1/i\nabla)$ means that we are to substitute $\partial/i\partial x_j$ for δk_j. The last term of Eq.(2.37) is transformed as

$$\begin{aligned} & \iint d^3q\ d^3k\ U(\mathbf{k}-\mathbf{q}) C_n(\mathbf{q}) e^{i\delta\mathbf{k}\cdot\mathbf{r}} \\ &= \frac{1}{(2\pi)^3} \iiint d^3q\ d^3k\ d^3r'\ U(\mathbf{r}') e^{i(\mathbf{k}-\mathbf{q})\cdot\mathbf{r}'} e^{i(\mathbf{k}-\mathbf{k}_o)\cdot\mathbf{r}'} C_n(\mathbf{q}) \end{aligned} \tag{2.42}$$

If $|\mathbf{r}|$ is large compared to a lattice spacing, the errors from approximation are not important for slowly varying impurity potentials. Therefore, we are able to simplify Eq.(2.42) as

$$\frac{1}{(2\pi)^3}\iiint d^3q\ d^3k\ d^3k\ e^{i\mathbf{k}\bullet(\mathbf{r}-\mathbf{r}')}e^{i\delta\mathbf{k}\bullet\mathbf{r}}U(\mathbf{r}')C_n(\mathbf{q}) = U(\mathbf{r})F_n(\mathbf{r}) \qquad (2.43)$$

Now, we have, in replace of Eq.(2.37)

$$\left(E_n\frac{1}{i\nabla}-E\right)F_n(\mathbf{r})+U(\mathbf{r})F_n(\mathbf{r})=0 \qquad (2.44)$$

This is the transformed effective mass equation and does not contain any terms coupling different bands.

Now, we introduce Wannier functions $a_n(\mathbf{r}-\mathbf{R}_\mu)$, characterized by a band index and a lattice site vector $\mathbf{R}_\mu$, to express the wave function in terms of orthogonal localized functions.

$$a_n(\mathbf{r}-\mathbf{R}_\mu)=\sqrt{\frac{\Omega}{(2\pi)^3}}\int e^{-i\mathbf{k}\bullet\mathbf{R}_\mu}\phi_n(\mathbf{k},\mathbf{r})d^3k \qquad (2.45)$$

After some algebra, the Bloch functions can be expressed as

$$\phi_n(\mathbf{q},\mathbf{r})=\sqrt{\frac{\Omega}{(2\pi)^3}}\sum_\mu e^{-i\mathbf{q}\bullet\mathbf{R}_\mu}a_n(\mathbf{r}-\mathbf{R}_\mu) \qquad (2.46)$$

With Eq.(2.46) and the transformation $C=e^{-iS}A$, we have

$$\begin{aligned}A_n(\mathbf{k}) &= \sum_l\int\left[n\mathbf{k}\left|e^{iS}\right|l\mathbf{q}\right]C_l(\mathbf{q})d^3q\\ &= C_n(\mathbf{k})-\frac{\delta\mathbf{k}}{m}\sum_l\frac{\mathbf{p}_{nl}}{\omega_{nl}}C_l(\mathbf{k})\end{aligned} \qquad (2.47)$$

where $\omega_{nl}=(E_n-E_l)/\hbar$. The leading term in A_n is just C_n, and we neglect the first-order correction. To this order

$$\begin{aligned}\varphi(\mathbf{r}) &= \sum_n\int C_n(\mathbf{k})e^{i(\mathbf{k}-\mathbf{k}_\circ)\bullet\mathbf{r}}\phi_n(\mathbf{k}_\mathbf{0},\mathbf{r})d^3k\\ &= \sum_n\phi_n(\mathbf{k}_\mathbf{0},\mathbf{r})F_n(\mathbf{r})\end{aligned} \qquad (2.48)$$

If we are interested in the wave function associated with a particular impurity level under the conduction band, for instance *n*=*c*, we have finally

$$\varphi(\mathbf{r}) = \phi_c(\mathbf{k_o}, \mathbf{r}) F(\mathbf{r}) \tag{2.49}$$

The impurity function is then an oscillatory band wave function modulated by a slowly varying, but exponentially decreasing, envelope function $F(\mathbf{r})$.

2-2-2 Effective mass theory in BECs

We, in turn, adopt the effective mass equation [Eq.(2.44)] to consider a Bose-Einstein condensate in an optical lattice, described by G-P equation. For the envelope functions vary not faster than on a scale of three lattice constants, the nonlinear terms should be added to Eq.(2.44) in a straightforward way

$$\left(E_n \frac{1}{i\nabla} - E\right) F_n(\mathbf{r}) + U(\mathbf{r}) F_n(\mathbf{r}) + \sigma \left|F_n(\mathbf{r})\right|^2 F_n(\mathbf{r}) = 0 \tag{2.50}$$

or

$$\left((E_n - E) + \sum \alpha_{ij} \frac{\partial}{i\partial x_i} \frac{\partial}{i\partial x_j}\right) F_n(\mathbf{r}) + U(\mathbf{r}) F_n(\mathbf{r}) + \sigma \left|F_n(\mathbf{r})\right|^2 F_n(\mathbf{r}) = 0 \tag{2.51}$$

where σ is the strength of the nonlinear interatomic interaction. x_i and x_j are cartesian components of $\mathbf{r}$. Finally, we have the transformed effective mass equation contains nonlinear interaction without coupling bands.

Now, we proceed to consider the nonlinear Schrödinger equation without external influence as in Eq.(2.3), the effective mass equation in Eq.(2.51) is rewritten as

$$-\frac{1}{2m_n^*} \frac{\partial^2 F_n(X)}{\partial X^2} - \delta_n F_n(X) + \sigma_n \left|F_n(X)\right|^2 F_n(X) = 0 \tag{2.52}$$

where $\delta_n \equiv E - E_n(k_o)$ is the detuning chemical potential from $E_n(k_o)$, the

chemical potential at the extreme point of the band. This is the effective-mass equation near the extreme points of the band, k_o , by making a unitary transformation to diagonalize the Hermitian matrix of Eq.(2.3). In deriving Eq.(2.52), we have assumed that the band mixing is small. If the band mixing is not negligible, a two-band model is necessary to describe BECs in optical lattices. We believe that $E_n(k_o)$ is usually ignored in the applications of the effective-mass theory [12], cannot be ignored and is important to describe BECs in optical lattices, qualitatively and quantitatively. The effective nonlinear interaction strength σ_n is given by

$$\sigma_n = \pi\sigma\int_{-1}^{1}\left|u_n\left(k_o, X\right)\right|^4 dX \tag{2.53}$$

The reciprocal effective mass is $1/m_n^* = \partial^2 E(k)/\partial k^2$ for band n as being defined in solid-state physics. With second-order differential of Eq.(2.14), effective mass m_a^* at E_a is given by

$$\frac{1}{m_a^*} = 1 - \frac{\pi^2}{V_o} \tag{2.54}$$

effective mass m_b^* at E_b is given by

$$\frac{1}{m_b^*} = 1 + \frac{\pi^2}{V_o} \tag{2.55}$$

and, effective mass m_c^* at E_c is given by

$$m_c^* = 1 \tag{2.56}$$

The effective mass can be positive or negative depending on the band. With proper atomic interaction σ_n and the detuning chemical potential δ_n, solitons may emerge from band edge $E_n(k_o)$.

Eq.(2.52) is a time-independent nonlinear Schrödinger equation governing the

condensate envelope function $F_n(X)$, which is related to the condensate wave function by $\varphi(X)=\sum_n \phi_n(k_o,X)F_n(X)$ from Eq.(2.49). If we are interested in the condensate wave function associated with a particular localized state developed from a certain band, from Eq.(2.49), we have

$$\varphi_n(X)=\phi_n(k_o,X)F_n(X) \tag{2.57}$$

where n is band index marked as a, b, or c in this thesis.

To give a brief summary, we have derived the condensate wave function of a time-independent nonlinear Schrödinger equation with a periodic potential to be an oscillatory band wave function modulated by a slowly varying envelope function $F_n(X)$. In next chapter, we introduce the bright and dark solitons arise from the BECs in optical lattices and discuss their properties.

2-3 Numerical Method

For obtaining the numerical results of one-dimensional G-P equation in Eq.(2.3) at steady state, we introduce numerical differentiation for approximating a second-order derivative, Newton-Raphson method for finding the solutions of nonlinear equations, and numerical integration for calculating the number of atoms in a BEC [Eq.(2.4)].

2-3-1 Numerical Differentiation

We use central-difference formula of order $O(h^2)$ as a second-order derivative

$f''(x)$. Start with the Taylor expansions

$$f(x+h)=f(x)+hf'(x)+\frac{h^2f''(x)}{2!}+\frac{h^3f^{(3)}(x)}{3!}+\frac{h^4f^{(4)}(x)}{4!}+\cdots \quad (2.58)$$

and

$$f(x-h)=f(x)-hf'(x)+\frac{h^2f''(x)}{2!}-\frac{h^3f^{(3)}(x)}{3!}+\frac{h^4f^{(4)}(x)}{4!}+\cdots \quad (2.59)$$

Adding the two Eqs.(2.58)(2.59), we have

$$f''(x)=\frac{f(x+h)-2f(x)+f(x-h)}{h^2}-\frac{2h^2f^{(4)}(x)}{4!}-\frac{2h^4f^{(6)}(x)}{6!}-\cdots \quad (2.60)$$

If the series in Eq.(2.60) is truncated at the fourth derivative, there exists a value c that lies in $[x-h,x+h]$ so that

$$f_o''=\frac{f_1-2f_o+f_{-1}}{h^2}-\frac{2h^2f^{(4)}(c)}{4!} \quad (2.61)$$

This gives us the desired formula for approximating $f''(x)$

$$f_o''\approx\frac{f_1-2f_o+f_{-1}}{h^2} \quad (2.62)$$

We consequently have the error h^2.

2-3-2 Newton-Raphson theorem [18]

We apply Newton-Raphson (or simply Newton's) method for finding the solutions of nonlinear equations. Assume that $f\in C^2[a,b]$ and there exists a number $p\in[a,b]$ where $f(p)=0$. If $f'(p)\neq 0$, then there exists a $\delta>0$ such that the sequence $\{p_k\}_{k=0}^{\infty}$ defined by the iteration

$$p_k=g(p_{k-1})=p_{k-1}-\frac{f(p_{k-1})}{f'(p_{k-1})} \quad \text{for } k=1,2,... \quad (2.63)$$

will converge to p for any initial approximation $p_o \in [p-\delta, p+\delta]$. The function $g(x)$ defined by the formula

$$g(x) = x - \frac{f(x)}{f'(x)} \tag{2.64}$$

is called the Newton-Raphson iteration function. Since $f(p) = 0$ it is easy to see that $g(p) = 0$. Thus, the Newton-Raphson iteration for finding the root of the equation $f(x) = 0$ is accomplished by finding a fixed point of the equation $g(x) = x$. Since Newton's method rely on the continuity of $f'(x) = 0$ and $f''(x) = 0$, we start with the Taylor polynomial of degree $n = 1$

$$f(x) = f(p_o) + f'(p_o)(x - p_o) + \frac{f''(c)(x - p_o)^2}{2!} \tag{2.65}$$

where c lies somewhere between p_o and x. Substituting $x = p$ into Eq.(2.65) and using the fact that $f(p) = 0$ produces

$$0 = f(p_o) + f'(p_o)(x - p_o) + \frac{f''(c)(x - p_o)^2}{2!} \tag{2.66}$$

If p_o is close enough to p, the last term on the right side of Eq.(2.66) will be small enough compared to the sum of the first two terms. Hence, it can be neglected and we can use the approximation

$$0 \approx f(p_o) + f'(p_o)(p - p_o) \tag{2.67}$$

Solving for p in Eq.(2.67), we get $p \approx p_o - f(p_o)/f'(p_o)$. This is used to define the next approximation p_1 to the root

$$p_1 = p_o - \frac{f(p_o)}{f'(p_o)} \tag{2.68}$$

When p_{k-1} is used in place of p_o in Eq.(2.68), the general rule Eq.(2.63) is established. For most applications this is all that needs to be understood. However, to fully comprehend what is happing we need to consider the fix-point iteration function. The key is in the analysis of $g'(x)$

$$g'(x)=\frac{f(x)f''(x)}{\left[f'(x)\right]^2}$$

Since $g'(p)=f(p)f''(p)\Big/\left[f'(p)\right]^2=0$ and $g(x)$ is continuous, it is possible to find a $\delta>0$ so that the hypothesis $\left|g'(x)\right|\le 1$ is satisfied on $\left[p-\delta,p+\delta\right]$. Therefore, a sufficient condition for p_o to initialize a convergent sequence $\{p_k\}_{k=0}^{\infty}$ which converges to a root of $f(x)=0$ is that $p_o\in\left[p-\delta,p+\delta\right]$ and that δ be chosen so that

$$\frac{\left|f(x)f''(x)\right|}{\left|f'(x)\right|^2}<1 \qquad \text{for all } x\in\left[p-\delta,p+\delta\right] \tag{2.69}$$

2-3-3 Numerical Integration [19]

We adopt a three-point formula exact up to polynomials of degree two. This is true; moreover, by a cancellation of coefficients due to left-right symmetry of the formula, the three-point formula is exact for polynomials up to and including degree three, i.e. $f(x)=x^3$. We have the Simpson's rule

$$\int_{x_1}^{x_3} f(x)dx=h\left[\frac{1}{3}f_1+\frac{4}{3}f_2+\frac{1}{3}f_3\right]+O\left(h^5f^{(4)}\right) \tag{2.70}$$

where $x_i=x_o+ih$; $i=0,1,\cdots,N+1$ and $f(x_i)\equiv f_i$. Here $f^{(4)}$ means the fourth derivative of the function f evaluated at an unknown place in the interval

and therefore the error is h^5. Note that the formula gives the integral over an interval of size $2h$, so the coefficients add up to two.

Chapter 3 Simulation Results and Discussion

We have applied the effective mass theory to the Gross-Pitaevskii (G-P) equation, nonlinear Schrödinger equation with optical lattices, to obtained the effective mass equation [Eq.(2.52)]

$$-\frac{1}{2m_n^*}\frac{\partial^2 F_n(X)}{\partial X^2}-\delta_n F_n(X)+\sigma_n\left|F_n(X)\right|^2 F_n(X)=0$$

The condensate wave function associated with a particular localized state developed from a certain band is shown in Eq.(2.57)

$$\varphi_n(X)=\phi_n(k_o,X)F_n(X)$$

which is an oscillatory band wave function $\phi_n(k_o,X)$ modulated by a slowly varying, but exponentially decreasing, envelope function $F_n(X)$ which provides a concrete picture to study the properties of BECs for certain energy in band structure. If the energy is within the band gap, gap solitons occur. These solitons, characterized by localized wavepackets of the condensates, are also called bright solitons. On the other hand, for the energy is within the band, dark solitons occur and are characterized by localized dips on the condensate density background.

In the following, we apply the effective mass equation to obtain the analytic solutions of bright and dark solitons, respectively. Both numerical simulations and experimental results reported by Eiermann *et al.* [20] are applied to confirm that this envelope function approach indeed provides us with useful qualitative insight into the condensate dynamics.

3-1 Bright Solitons

For the energy is within band gap, bright soliton solutions can be described by the envelope functions which satisfy effective mass equation [Eq.(2.52)] and are given by

$$F_n(X) = A_n \operatorname{sech}(B_n X) \tag{3.1}$$

where $B_n = \sqrt{2\left|\delta_n m_n^*\right|}$ and $A_n = B_n \Big/ \sqrt{\left|m_n^* \sigma_n\right|}$. Bright solitons are developed from states of the upper (lower) band edge of the band gap, if atomic interactions are attractive (repulsive). The sign of detuning chemical potential, atomic interactions and effective mass determines whether bright solitons exist or not. For the energy is below the band edge $\delta_n < 0$, the effective mass $m_n^* > 0$, and attractive atomic interactions $\sigma_n < 0$. For the energy is above the band edge $\delta_n > 0$, the effective mass $m_n^* < 0$, and repulsive atomic interactions $\sigma_n > 0$. From Eq.(3.1), we know that the gap soliton width is inversely proportional to B_n and depends upon the detuning chemical potential δ_n, which is the relative chemical potential to the band edges. The properties of a gap soliton are determined by δ_n, therefore, in order to understand BECs in optical lattices qualitatively and quantitatively, the chemical potential $E_n(k_o)$ at band edge is significant. Near the band edge, where $\left|\delta_n\right|$ and B_n are small, the soliton is much extended (occupying many lattice sites) in the space and decay slowly to infinity. Deep inside the band gap, where $\left|\delta_n\right|$ and B_n are large, the soliton is much confined in the space. These analytic soliton properties are consistent with the numerical studies of BECs in optical lattices [8, 10].

We proceed to add oscillatory Bloch waves $\phi_n(k_o, X)$ to envelope function

$F_n(X)$ to obtain the condensate wave functions. According to the states in the band from which solitons are developed, we classify gap solitons into categories that are Bragg-reflection type and internal-reflection type, respectively. Note that we kept the depth of the optical lattices $V_o = 2.5$ in our numerical studies.

3-1-1 Bragg-Reflection Type

Solitons which arise from the energy E_a, the first band at $k = \pi/2$, or E_b, the second band at $k = \pi/2$, are classified in Bragg-Reflection Type. From Eq. (2.15) and Eq. (2.16), we have $E_a = 1.859$ and $E_b = 3.109$, respectively. For the solitons arising from E_a, we have the energy goes up to the second band gap which implies $\delta_a > 0$, the effective mass $m_a^* = -0.339$ [Eq.(2.54)] is negative, and the formation of gap solitons is under repulsive atomic interactions $\sigma > 0$. For convenience, we name gap solitons which arise from E_a as a-type gap solitons. By multiplying the Bloch wave $\phi_a(X, \pi/2) = \sqrt{1/\pi}\cos(\pi/2\,X)$ [Eq.(2.17)] to the envelope function of Eq.(3.1), the condensate wave function of gap solitons developed from E_a is given by

$$\varphi_a(X) = A\ \mathrm{sech}(BX)\frac{1}{\sqrt{\pi}}\cos\left(\frac{\pi X}{2}\right) \tag{3.2}$$

We plot a series of the typical a-type gap solitons which are developed from the first band edge for repulsive atomic interactions for different energy under $V_o = 2.5$. These plots are Fig. 2(a), Fig. 2(b) and Fig. 2(c) which correspond to the energy $E = 2.015$, $E = 2.4837$, and $E = 2.9525$, respectively. They have even symmetric Bloch wave under soliton envelope. For comparison, we numerically solve time-independent G-P equation [Eq.(2.3)] and plot in Fig. 2(d), Fig. 2(e) and Fig. 2(f)

for the a-type gap solitons at the corresponding energies.

On the other hand, for the solitons arising from E_b, we have the energy goes down to the second band gap which implies $\delta_b < 0$, the effective mass $m_b^* = 0.202$ [Eq.(2.55)] is positive, and the formation of gap solitons is under attractive atomic interactions $\sigma < 0$. For convenience, we name gap solitons which arise from E_b as b-type gap solitons. By multiplying the Bloch wave $\phi_b(X, \pi/2) = \sqrt{1/\pi}\sin(\pi/2\,X)$ [Eq.(2.18)] to the envelope function of Eq.(3.1), the wave function of gap solitons developed from E_b is given by

$$\varphi_b(X) = A\ \mathrm{sech}(BX)\frac{1}{\sqrt{\pi}}\sin\left(\frac{\pi X}{2}\right) \tag{3.3}$$

We plot a series of the typical b-type gap solitons which are developed from the second band edge for attractive atomic interactions for different energy under $V_o = 2.5$. These plots are Fig. 3(a), Fig. 3(b) and Fig. 3(c) which correspond to the energy $E = 2.015$, $E = 2.4837$, and $E = 2.9525$, respectively. They have odd symmetric Bloch wave under soliton envelope. For comparison, we again numerically solve time-independent G-P equation [Eq.(2.3)] and plot in Fig. 3(d), Fig. 3(e) and Fig. 3(f) for the b-type gap solitons at the corresponding energies.

The results of a-type and b-type gap solitons reveal high agreement between the analytic and numerical solutions, especially, when detuning chemical potential $|\delta_n|$ is small. The oscillations of gap solitons are due to the cosine and sine standing wave functions at the E_a and E_b as the Bragg reflection (BR) type solitons. They are the modulated standing Bloch waves, resulting from the interference of counter-propagating Bragg reflected waves, by the soliton envelope

function.

To obtain the analytic particle number N related to the detuning chemical potential δ_a for the a-type gap solitons, we substitute Eq.(3.2) into the conservation of number of atoms in Eq.(2.4)

$$N = \frac{1}{\pi}\left(\frac{A^2}{B} + \frac{A^2\pi^2}{2B^2}\operatorname{csch}\left(\frac{\pi^2}{2B}\right)\right) \tag{3.4}$$

To obtain the analytic particle number N related to the detuning chemical potential δ_b for the b-type gap solitons, we substitute Eq.(3.3) into the conservation of number of atoms in Eq.(2.4)

$$N = \frac{1}{\pi}\left(\frac{A^2}{B} - \frac{A^2\pi^2}{2B^2}\operatorname{csch}\left(\frac{\pi^2}{2B}\right)\right) \tag{3.5}$$

The number of atoms N in a BEC at different energies for a-type and b-type gap solitons are plotted in Fig. 5. From Eq.(3.4) and Eq.(3.5), we found the atomic number N is approximately proportional to $\sqrt{|\delta|}$ and it is small close to the band edges and becomes zero at band edges. These properties are not only consistent with the numerical simulations [10, 11] but also with our simulations as shown in Fig. 5. Going deeper inside the band gap, the particle number N becomes large and the nonlinear effect is strong (solitons being more localized).

3-1-2 Internal-Reflection Type

Solitons which arise from the energy E_c, the first band at $k = 0$ are classified in Internal-Reflection Type. From Eq.(2.21), we have $E_c = 1.096$. For the solitons arising from E_c, we have the energy goes down to the first band gap which implies

$\delta_c < 0$, the effective mass $m_c^* = 1$ [Eq.(2.56)] is positive, and the formation of gap solitons is under attractive atomic interactions $\sigma < 0$. For convenience, we name gap solitons arise from E_c as *c*-type gap solitons. By multiplying the Bloch wave $\phi(X,0) = (b_o + b_{-1}\cos\pi X)$ [Eq.(2.19)] to the envelope function of Eq.(3.1), the wave function of gap solitons developed from E_c is given by

$$\varphi_c(X) = A\ \mathrm{sech}(BX)(b_o + b_{-1}\cos\pi X) \tag{3.6}$$

We plot a series of the typical *c*-type gap solitons as shown in Fig. 4(a), Fig. 4(b) and Fig. 4(c) which correspond to the energy $E = 0.1371$, $E = 0.5482$, and $E = 0.9594$, respectively. For comparison, we again numerically solve time-independent G-P equation [Eq.(2.3)] and plot in Fig. 4(d), Fig. 4(e) and Fig. 4(f) for the *c*-type gap solitons at the corresponding energies. Note that the Bloch wave function is no longer a standing wave due to no coupling with counter-propagating wave. The soliton is mainly localized by the attractive potential rather than by Bragg reflection in the periodic structure; in this band, it resembles an ordinary guided wave modulated by a periodic structure and acts as internal reflection (IR) wave which does not contain zeros. It is a fundamental eigenmode gap soliton with small ripples and it becomes pure sech^2 profile for the soliton energy deeper in the gap or with lower soliton energy.

To obtain the analytic particle number N related to the detuning chemical potential δ_c for the *c*-type gap solitons, we substitute Eq.(3.6) into the conservation of number of atoms in Eq.(2.4)

$$N = A^2\left(\frac{1}{\pi B} + \frac{2ab\pi^2}{B^2}\mathrm{csch}\left(\frac{\pi^2}{2B}\right) + \frac{b^2\pi^2}{B^2}\mathrm{csch}\left(\frac{\pi^2}{B}\right)\right) \tag{3.7}$$

where the coefficients a, b are given by

$$\begin{pmatrix} a \\ b \end{pmatrix} = \frac{1}{\sqrt{2\pi}\sqrt{\pi^4 + 2V_o^{\,2} - \pi^2\sqrt{\pi^4 + 2V_o^{\,2}}}} \begin{pmatrix} V_o \\ \sqrt{\pi^4 + 2V_o^{\,2}} - \pi^2 \end{pmatrix} \tag{3.8}$$

Number of atoms in condensates N is also approximately proportional to $\sqrt{|\delta|}$ and does not exhibit atomic population cutoffs at band edge as shown in Fig. 5. It becomes large as the localized state goes deeper inside the band gap where the nonlinear effect is strong (solitons being more localized). However, we found in Fig. 5 the numerical particle numbers of *a*-type and *b*-type both slightly larger than those obtained from the analytic formula of Eq.(3.4) and Eq.(3.5), but that for *c*-type is smaller.

3-2 Dark Solitons

For the energy is on the band, dark soliton solutions can be described by the envelope functions which satisfy effective mass equation [Eq.(2.52)] and are given by

$$F_n(X) = A_n \tanh(B_n X) \tag{3.9}$$

where $B_n = \sqrt{|\delta_n m_n^*|}$ and $A_n = B_n \Big/ \sqrt{|m_n^* \sigma_n|}$. Dark solitons are developed from states of the upper (lower) band edge of the band gap, if atomic interactions are repulsive (attractive). The sign of detuning chemical potential, atomic interactions and effective mass determines whether dark solitons exist or not. For the energy is above the band edge $\delta_n > 0$, the effective mass $m_n^* > 0$, and repulsive atomic interactions $\sigma_n > 0$. For the energy is below the band edge $\delta_n < 0$, the effective mass $m_n^* < 0$, and attractive atomic interactions $\sigma_n < 0$. The atomic interaction of dark solitons is contrary to that of bright solitons while sign of the effective mass remains the same. From Eq.(3.9), we know that width of dark soliton is inversely

proportional to B_n and the background condensate density is proportional to A_n. These two properties both depend upon the detuning chemical potential δ_n, which is the relative chemical potential to the band edges. Near the band edge, where $|\delta_n|$, B_n and A_n are small, the width of the localized condensate density dips is extended (occupying many lattice sites) in the space and the background condensate density is low. Deep inside the band, where $|\delta_n|$, B_n and A_n are large, width of the dips is much confined and the background density is high. We find that he chemical potential $E_n(k_o)$ at band edge plays an important role in order to study BECs in optical lattices qualitatively and quantitatively. To confirm these properties of dark solitons, we solve the condensate wave functions analytically and numerically.

The procedure to seek for the condensate wave functions of dark solitons is analogous to that of bright solitons and is to add oscillatory band wave function $\phi_n(k_o, X)$ to envelope function $F_n(X)$. According to the states on the band from which solitons are developed, we classify gap solitons into categories that are the Bragg-reflection type and internal-reflection type, respectively. Note that we kept the depth of the optical lattices $V_o = 2.5$ in the numerical studies.

3-2-1 Bragg-Reflection Type

Same as for dark solitons which arise from the energy E_a, the first band at $k = \pi/2$, or E_b, the second band at $k = \pi/2$, are classified in Bragg-Reflection Type. For dark solitons arising from the energy $E_a = 1.859$, we have the detuning chemical potential $\delta_a < 0$ and negative effective mass $m_a^* = -0.339$ [Eq.(2.54)]. The

atomic interaction to form dark solitons is turned into attractive $\sigma < 0$ while the effective mass leaves unchanged. For convenience, we call dark solitons arise from E_a as a-type dark solitons. By multiplying the Bloch wave $\phi_a(X,\pi/2) = \sqrt{1/\pi}\cos(\pi/2\,X)$ [Eq.(2.17)] to the envelope function of Eq.(3.9), the wave function of dark solitons developed from E_a is given by

$$\varphi_a(X) = A\tanh(BX)\frac{1}{\sqrt{\pi}}\cos\left(\frac{\pi X}{2}\right) \tag{3.10}$$

We plot a series of the typical a-type dark solitons as shown in Fig. 6(a), Fig. 6(b) and Fig. 6(c) which correspond to the energy $E = 1.1917$, $E = 1.4776$, and $E = 1.7634$, respectively. For comparison, we numerically solve time-independent G-P equation [Eq.(2.3)] and plot in Fig. 6(d), Fig. 6(e) and Fig. 6(f) for the a-type dark solitons at the corresponding energies.

For dark solitons arising from the energy $E_b = 3.109$, we have the detuning chemical potential $\delta_b > 0$ and positive effective mass $m_b^* = 0.202$ [Eq.(2.55)]. The atomic interaction to form dark solitons is turned into repulsive $\sigma > 0$ and the effective mass leaves unchanged. For convenience, we call dark solitons arise from E_b as b-type dark solitons. By multiplying the Bloch wave $\phi_b(X,\pi/2) = \sqrt{1/\pi}\sin(\pi/2\,X)$ [Eq.(2.18)] to the envelope function of Eq.(3.9), the wave function of dark solitons developed from E_b is given by

$$\varphi_b(X) = A\tanh(BX)\frac{1}{\sqrt{\pi}}\sin\left(\frac{\pi X}{2}\right) \tag{3.11}$$

We plot a series of the typical b-type dark solitons as shown in Fig. 7(a), Fig. 7(b) and Fig. 7(c) which correspond to the energy $E = 3.204$, $E = 3.4898$, and $E = 3.7757$, respectively. For comparison, we numerically solve time-independent G-P equation [Eq.(2.3)] and plot in Fig. 7(d), Fig. 7(e) and Fig. 7(f) for the b-type dark solitons at the corresponding energies.

The results of a-type and b-type dark solitons reveal high agreement between the analytic and numerical solutions. Also, we show that the smaller detuning chemical potential $|\delta_n|$, the higher accuracy of the analytic results. Lower accuracy of the analytic results occurs around the position $X = 0$. The oscillations of a-type and b-type dark solitons are due to the cosine and sine standing wave functions at the E_a and E_b as the Bragg reflection (BR) type solitons. They are the modulated standing Bloch waves, resulting from the interference of counter-propagating Bragg reflected waves, by the soliton envelope function.

3-2-2 Internal-Reflection Type

For dark solitons arising from the energy $E_c = 1.096$ at $k = 0$ are classified as Internal-Reflection Type. We have the detuning chemical potential $\delta_c > 0$ and positive effective mass $m_c^* = 1$ [Eq.(2.56)]. The atomic interaction to form dark solitons is turned into repulsive $\sigma > 0$ and still the effective mass leaves unchanged. For convenience, we name dark solitons arise from E_c as c-type dark solitons. By multiplying the Bloch wave $\phi(X,0) = (b_o + b_{-1}\cos\pi X)$ [Eq.(2.19)] to the envelope function of Eq.(3.9), the wave function of dark solitons developed from E_c is given by

$$\varphi_c(X) = A\tanh(BX)(b_o + b_{-1}\cos\pi X) \tag{3.12}$$

We plot a series of the typical c-type dark solitons as shown in Fig. 8(a), Fig. 8(b) and Fig. 8(c) which correspond to the energy $E = 1.1917$, $E = 1.4776$, and $E = 1.7634$, respectively. For comparison, we again numerically solve time-independent G-P equation [Eq.(2.3)] and plot in Fig. 8(d), Fig. 8(e) and Fig. 8(f)

for the c-type dark solitons at the corresponding energies.

Mechanism of the formation of dark solitons is quite different from bright solitons. Condensate waves can propagate in linear regime since the energy of dark soliton is in band. With the consideration of atomic interaction, i.e., under nonlinear regime, phase difference $\Delta\theta$ between the parts left and right to the dark soliton (DS) plane, a plane of minimum condensate density, is π. This phase difference can be regarded as destructive interference of two waves, and hence there exist a localized dip in condensate density. In aspect of energy band spectrum, since the energy band structure shift slightly, there exist the nonlinear localized mode, dip on condensate density, i.e. dark solitons. Therefore, a dark soliton can propagate and its shape leave unchanged. Dark solitons are characterized by the dependence of a complementary norm N_c of the condensate wave function on the chemical potential E to represent a notch on the condensate density. We have N_c

$$N_c = \int \left[\varphi^2_{\text{background}}(X) - \varphi^2_{\text{soliton}}(X) \right] dX$$

where N_c represents a deficit of the condensate atoms associated with the formation of a dark soliton notch in the Bloch wave background. We analytically calculate the number of deficient atoms in condensate, N_c which are plotted in Fig. 9. The quantitative measure of this deficit depends on the width of the notch and the peak density of the background. As a rule, wider solitons form on lower density Bloch waves near the lower edges of spectral bands. The higher density nonlinear Bloch waves, corresponding to large chemical potentials, carry narrower dark states.

We have numerically and analytically demonstrated that bright (dark) solitons developed from both of band edges of the first and second bands at $k = \pi/2$ into the

second band gap (within the first band) are Bragg reflection type, a standing wave of counter propagating Bragg reflected Bloch waves due to optical lattices, whereas, bright (dark) soliton below the first band (within the first band) is mainly localized by the nonlinear attractive (repulsive) potential rather than by Bragg reflection in optical lattices. It resembles the ordinary guided waves modulated by a periodic structure and has internal reflection (IR) wave profile which does not contain zeros.

The first experimental observation of bright matter wave solitons with repulsive interaction for ^{87}Rb in optical lattices was reported by Eiermann *et al.* [20]. The experimental conditions are transverse and longitudinal trapping frequencies $\omega_{\perp} = 2\pi \times 85$ Hz and $\omega_{\parallel} = 2\pi \times 0.5$ Hz, and a standing light wave of wavelength $\lambda = 783$ nm. They deduced a soliton width of $x_o = 6$ μm from the absorption images and the inverse effective mass $1/m_a^* = -0.1$ from the experimentally measured soliton period, and they found the number of atoms is around 300. We proceed to compare our analytic results for *a*-type gap solitons with Eiermann's experimental results. We can, on the contrary, obtain the analytic bright solitons solutions by deducing the depth of the optical lattice $V_o = 0.8972$ from the effective mass $1/m_a^* = -0.1$ and the detuning chemical potential $\delta = 5.322 \times 10^{-3}$ from the soliton width $x_o = 6$ μm. Note that the soliton solutions are dimensionless and satisfy the effective one-dimensional G-P equation [Eq.(2.3)]. With parameter transformation discussed in Chapter 2, we can obtain solitons solutions satisfying one-dimensional G-P equation [Eq.(2.2)] instead and derive the number of atoms in bright soliton in dimensional variables

$$\boldsymbol{N} = \int |\psi|^2 dx = \int \frac{L}{2L_1} |\varphi|^2 dX = \int \frac{\hbar}{\omega_\perp a_s m L} |\varphi|^2 dX = \frac{\hbar}{\omega_\perp a_s m L} N \qquad (3.13)$$

where the lattice constant $L = \lambda/2$ and N is the number of atoms in dimensionless variables [Eq.(2.4)]. By substituting all parameters into Eq.(3.13), $\boldsymbol{N}$ is found to be 287 which well agree with Eiermann's experimental results. Eiermann's experiments show that only partial condensate atoms can form bright solitons and the rest condensate atoms are regarded as background. In aspect of our analytic soliton solutions, the detuning potential δ represents number of condensate atoms to form bright solitons, whereas the band edge energy $E_n(k_o)$ is regarded as background condensate atoms. For further discussion, we consider the product of atom number and soliton width as a function of the effective mass varied by adjusting the depth of the periodic potential. As the δ is small, the second term in Eq.(3.4) is negligible and we found that the product of soliton width and the number of atoms is proportional to the inverse effective mass. These results are shown in Fig.10 and are compared with Eiermann's experimental results [22]. Good coincidence between analytic solutions and experimental results is also revealed in Fig. 10. However, the foregoing are under small δ and V_o. To complete our discussion, we plot numerical and analytical N-E for $V_o = 1.5$ and $V_o = 3.5$ shown in Fig. 11(a) and Fig. 11(b), respectively. For small δ, the numerical and analytical results are in good agreement for both two values of V_o; for large δ, it is found that $V_o = 3.5$ has higher disagreement than $V_o = 1.5$. For large depth of the optical lattice, $V_o = 3.5$, the atoms are much confined in optical lattices, and hence the Bloch functions are not adequate to describe condensate atoms near band edge. Consequently, the inaccuracy of the analytic soliton solutions occurs. In summary, the effective mass theory can describe BECs in optical lattices qualitatively and quantitatively, especially adequate for small optical lattice and detuning potential.

Chapter 4 Conclusion and Perspective

4-1 Conclusion

We have applied the effective mass theory to study the dynamics of Bose-Einstein condensates (BECs) in optical lattices with either attractive or repulsive atom interactions. The macroscopic condensate wave function is describes by Gross-Pitaevskii (G-P) equation. We have derived the analytic soliton solution near band edge by including band edge energy as a parameter of solitons. The analytic soliton solution is found to be a Bloch function from the periodicity modulated by a soliton envelope function of the effective mass equation in which the periodic external potential appears in the form of an effective mass. The band edge energy is regarded as background condensate atoms at a specific wave vector to form solitons. We have demonstrated that the analytic soliton solutions can be either bright or dark solitons for both attractive and repulsive atom interactions since the energy band structure can change the dispersion of the BEC wavepackets dramatically. Both bright and dark solitons corresponding to energy in band gap and energy within band, respectively, can be categorized as Bragg reflection type solitons due to a standing wave of counter propagating Bragg reflected Bloch waves and internal reflection type solitons due to mainly localized by the attractive (repulsive) potential. The relation between the number of atoms to form solitons and energy has also been studied. As the energy goes deep inside the energy band (energy band gap), the number of atoms in dark (bright) soliton increases. Numerically solved the G-P equation, we confirmed the analytic soliton solutions agree reasonably well with simulations. The higher accuracy occurs at smaller detuning chemical potential and smaller depth of optical lattice. Eventually, we compared our bright soliton solutions with repulsive

interaction with the experimental results reported by Eiermann *et al.* [20]. Good agreement has been revealed. In conclusion, we have demonstrated that the band edge energy has physical significance to describe BECs in optical lattices and we have found that BECs in optical lattices can be described, qualitatively and quantitatively, by the effective-mass theory.

4-2 Perspective

We have applied the effective mass theory to study the stationary state BECs in optical lattices, i.e., the time-independent G-P equation throughout the Thesis and have showed that BECs in optical lattices can be described, qualitatively and quantitatively, by the effective-mass theory. In the future work, we can consider the time-dependent G-P equation where many phenomena of BECs in optical lattices can be experimentally demonstrated and/or theoretically investigated. The prediction of modulational instability (MI) [21] is one of the phenomena. Under the MI condition, the wavevector has imaginary term after adding a small perturbation wave to the Bloch wave and, consequently, the wave "grows up". In other words, solitons can occur under such condition. Konotop and Salerno [22] have studied the modulational instability in BECs in optical lattices by means of multiple-scale expansion. With such analysis, they obtain the velocity and inverse effective mass of the energy band, and explain the relation between the existence of solitons and the scattering length a_s. We can instead proceed to study MI of BECs in optical lattices by applying the effective mass theory to the time-dependent G-P equation.

References

[1] C. Salomon, J. Dalibard, A. Aspect, H. Metcalf, and C. Cohen-Tannoudji, *Phys. Rev. Lett.* **59**, 1659 (1987).

[2] B.P. Anderson and M.A. Kasevich, *Science* **282**, 1686 (1998).

[3] F.S. Cataliotti, S. Burger, C. Fort, P. Maddaloni, F. Minardi, A. Trombettoni, A . Smerzi, M. Inguscio, *Science* **293**, 843 (2001).

[4] J. H. Denschlag, J. E. Simsarian, H. H¨affner, C. McKenzie, A. Browaeys, D. Cho, K. Helmerson, S. L. Rolston, and W. D. Phillips, *J. Phys. B: At. Mol. Opt. Phys.* **35**, 3095 (2002).

[5] M. Cristiani, O. Morsch, J. H. M¨uller, D. Ciampini, and E. Arimondo, *Phys. Rev. A* **65** 063612 (2002).

[6] D. I. Choi and Q. Niu, *Phys. Rev. Lett.* **82**, 2022 (1999).

[7] D. N. Christodoulides and R. I. Joseph, *Phys. Rev. Lett.* **62**, 1746 (1989).

[8] C. C. Bradley, C. A. Sackett, and R. G. Hulet, *Phys. Rev. Lett.* **78**, 985 (1997).

[9] A. Trombettoni and A. Smerzi, *Phys. Rev. Lett.* **86**, 2353 (2001).

[10] P. J. Y. Louis, E. A. Ostrovskaya, C. M. Savage, and Y. S. Kivshar, *Phys. Rev. A* **67**, 013602 (2003).

[11] N. K. Efremidis and D. N. Christodoulides, *Phys. Rev. A* **67**, 063608 (2003).

[12] H. Pu, L. O. Baksmaty, W. Zhang, N. P. Bigelow, and P. Meystre, *Phys. Rev. A* **67**, 043605 (2003).

[13] S.F. Mingaleev and Yu.S. Kivshar, *Phys. Rev. Lett.* **86**, 5474 (2001).

[14] R. Slusher and B. Eggleton, eds., *Nonlinear Photonic Crystals* (Springer-Verlag, Berlin, 2003).

[15] Yu.S. Kivshar and G.P. Agrawal, *Optical Solitons: From Fibers to Photonic Crystals* (Academic Press, San Diego, 2003).

[16] F. Dalfovo, S. Giorgini, L. P. Pitaevskii, and S. Stringari, *Rev. Mod. Phys.* **71**, 463 (1999).

[17] Callaway, *Quantum Theory of the Solid State* (Academic Press, New York, 1991).

[18] J. H. Mathews, *Numerical Methods for Mathematics, Science, and Engineering* (Prentice-Hall, London, 1992).

[19] W. H. Press, S. A. Teukolsky, W. T. Vetterling and B. P. Flannery, *Numerical Recipes in C* (Cambridge University, New York, 1997).

[20] B. Eiermann, Th. Anker, M. Albiez, M. Taglieber, P. Treutlein, K.-P. Marzlin, and M.K. Oberthaler, *cond-mat* 0402178 (2004).

[21] F. Kh. Abdullaev, B. B. Baizakov, S. A. Darmanyan, V. V. Konotop, and M. Salerno, *Phys. Rev. A* **64**, 043606 (2001).

[22] V. V. Konotop, and M. Salerno, *Phys. Rev. A* **65**, 021602 (2002).

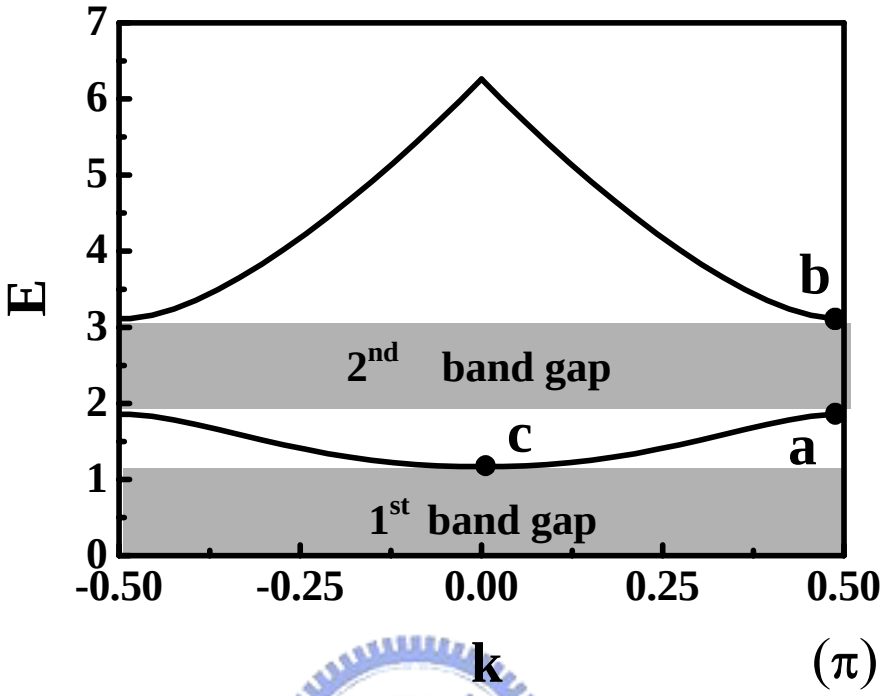

Fig. 1 Typical energy band spectrum $E-k$ of BECs for depth of optical lattices $V_o = 2.5$. Points "a" and "b" are the band edges of the first and second bands at $k = \pi/2$ and point "c" is the lowest band edge at $k = 0$. The shaded regions are the first and second band gap, respectively.

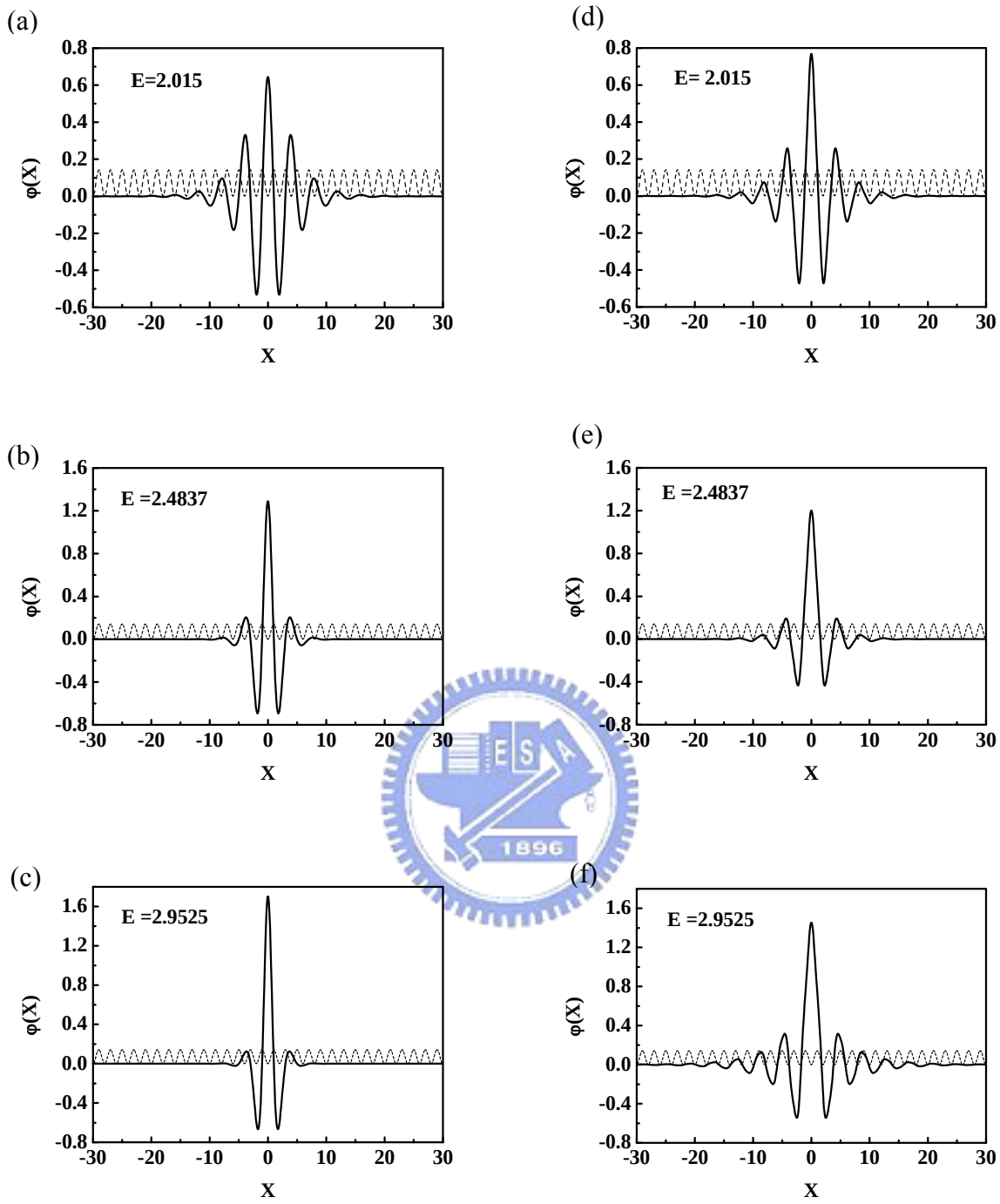

Fig. 2 *a*-type bright soliton for analytic result of $\varphi_a(X) = A\,\mathrm{sech}(BX)\frac{1}{\sqrt{\pi}}\cos\left(\frac{\pi X}{2}\right)$ with energy (a) $E = 2.015$, (b) $E = 2.4837$, and (c) $E = 2.9525$ and for the numerical result of G-P equation (d), (e), and (f). The dashed line represents optical lattices.

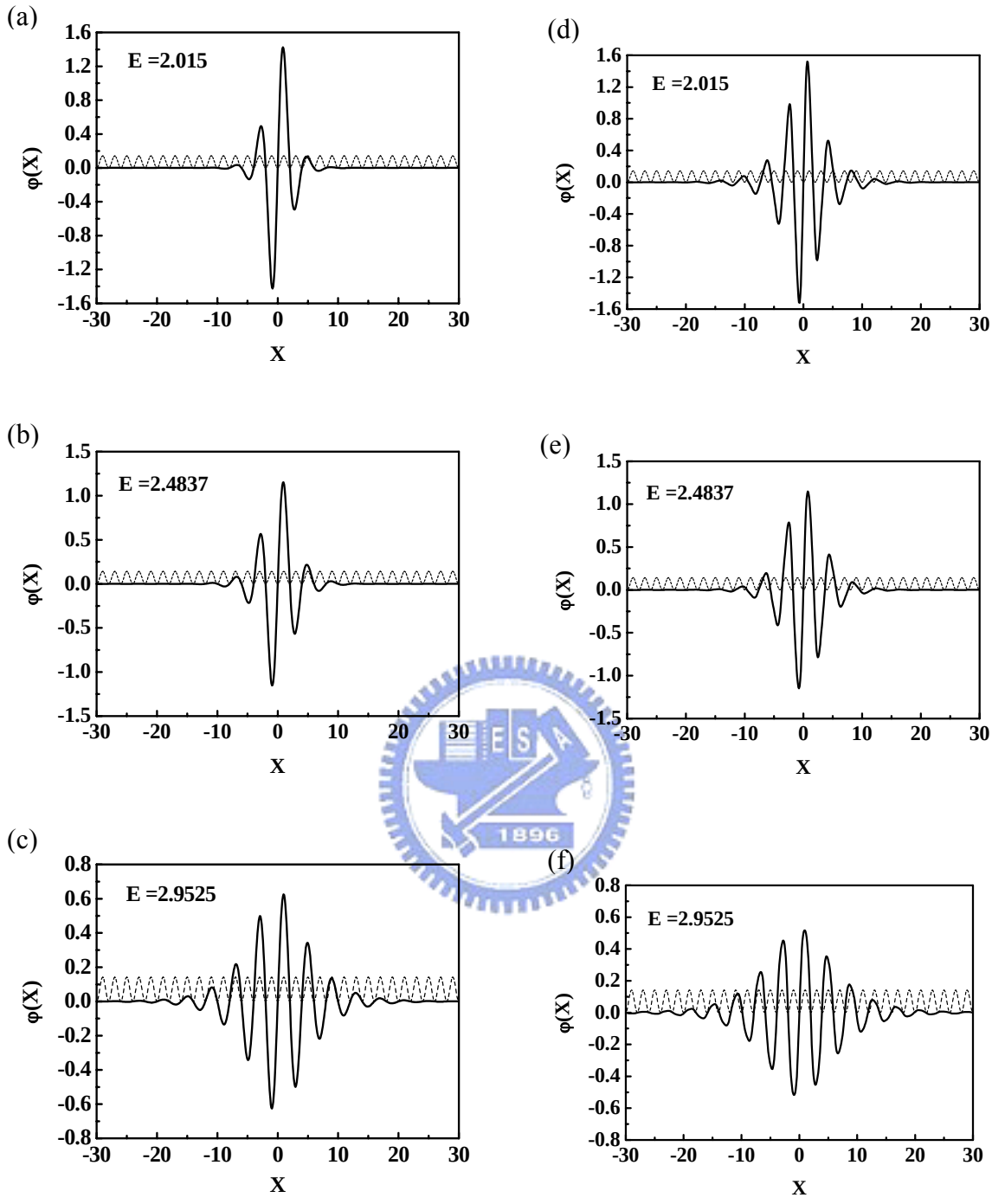

Fig. 3 *b*-type bright soliton for analytic result of $\varphi_b(X) = A\,\mathrm{sech}(BX)\frac{1}{\sqrt{\pi}}\sin\left(\frac{\pi X}{2}\right)$ with energy (a) $E = 2.015$, (b) $E = 2.4837$, and (c) $E = 2.9525$ and for the numerical result of G-P equation (d), (e), and (f). The dashed line represents optical lattices.

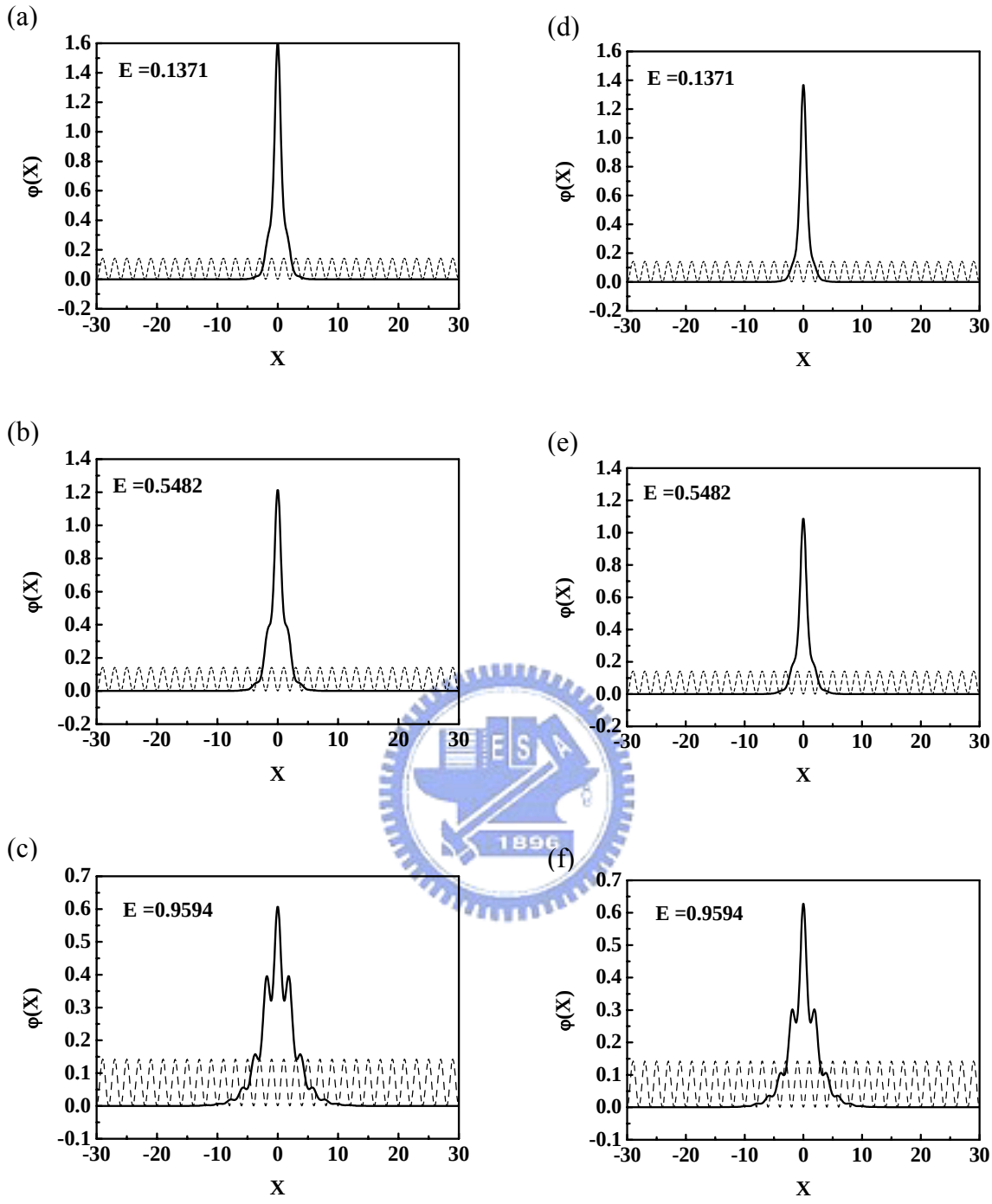

Fig. 4 *c*-type bright soliton for analytic result of $\varphi_c(X) = A\,\mathrm{sech}(BX)(b_o + b_{-1}\cos\pi X)$ with energy (a) $E = 0.1371$, (b) $E = 0.5482$, and (c) $E = 0.9594$ and for the numerical result of G-P equation (d), (e), and (f). The dashed line represents optical lattices.

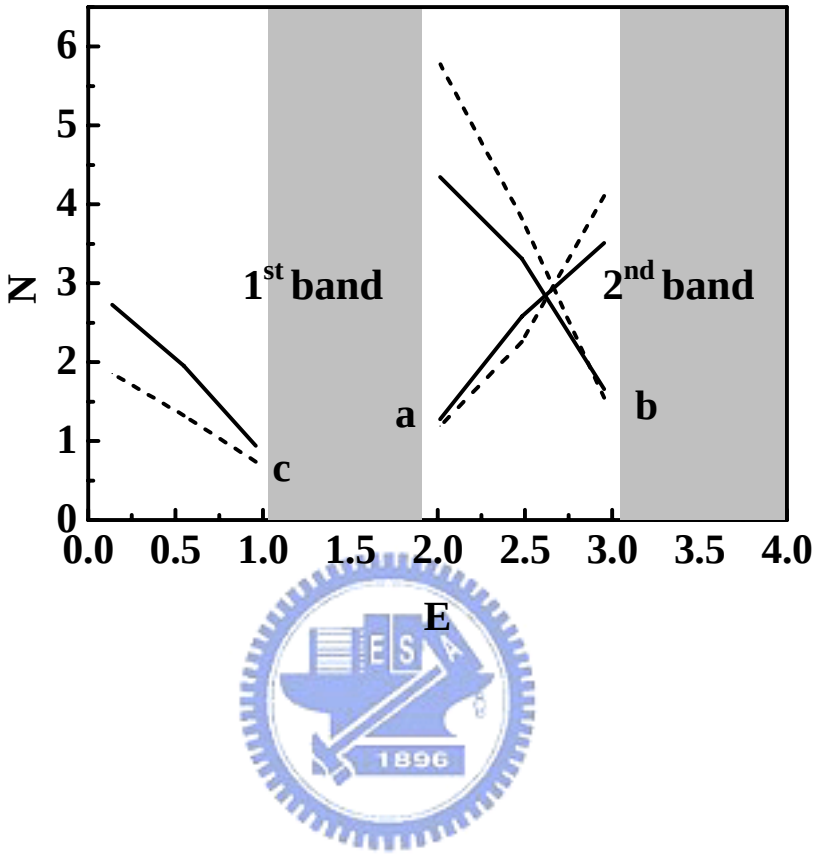

Fig. 5 Number of atoms in bright soliton N as a function of energy E for a-type, b-type and c-type. The solid and dashed curves are the analytic and numerical results, respectively. The shaded regions are the first and second band, respectively.

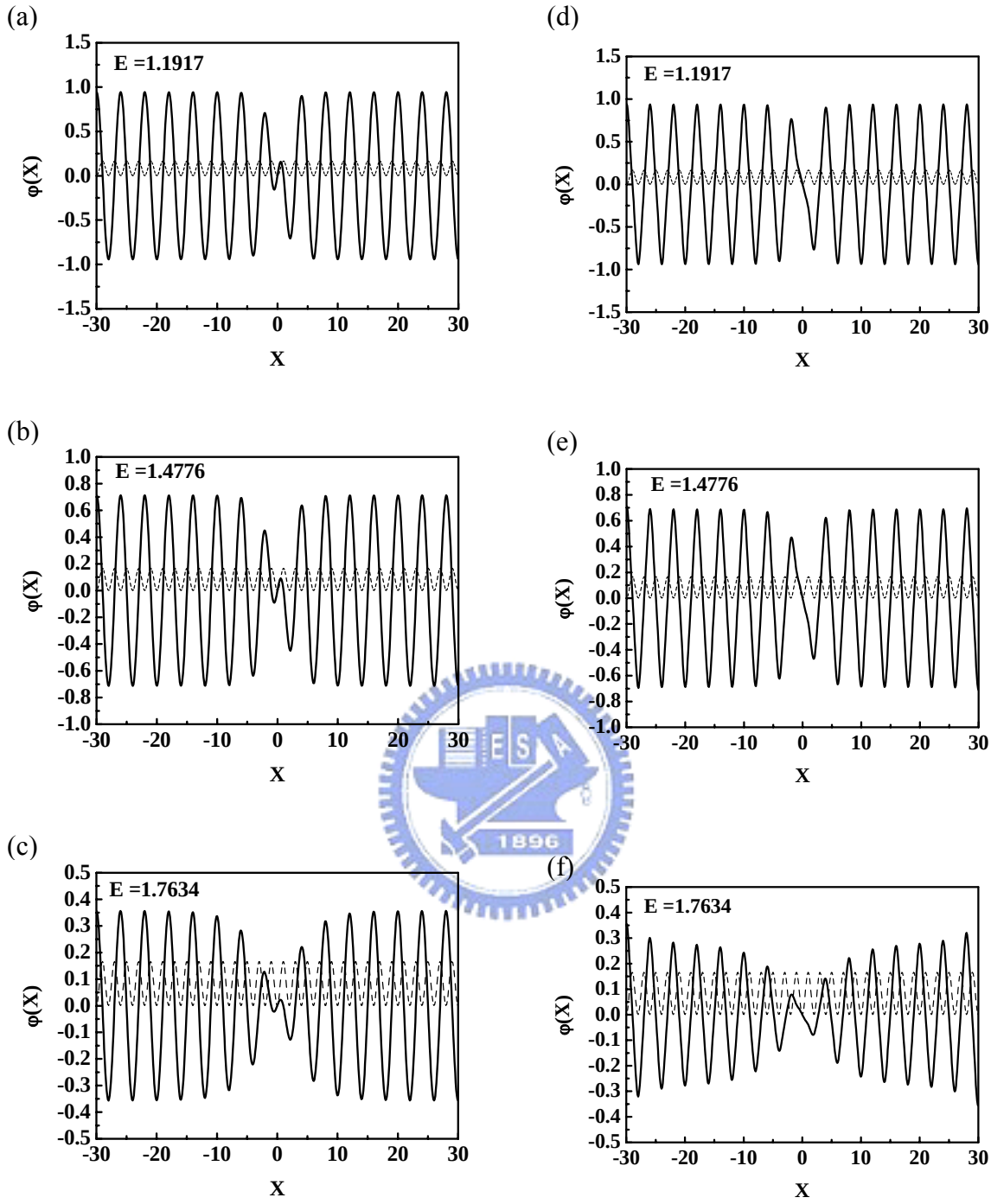

Fig. 6 a-type dark soliton for analytic result of $\varphi_a(X) = A\tanh(BX)\frac{1}{\sqrt{\pi}}\cos\left(\frac{\pi X}{2}\right)$ with energy (a) $E = 1.1917$, (b) $E = 1.4776$, and (c) $E = 1.7634$ and for the numerical result of G-P equation (d), (e), and (f). The dashed line represents optical lattices.

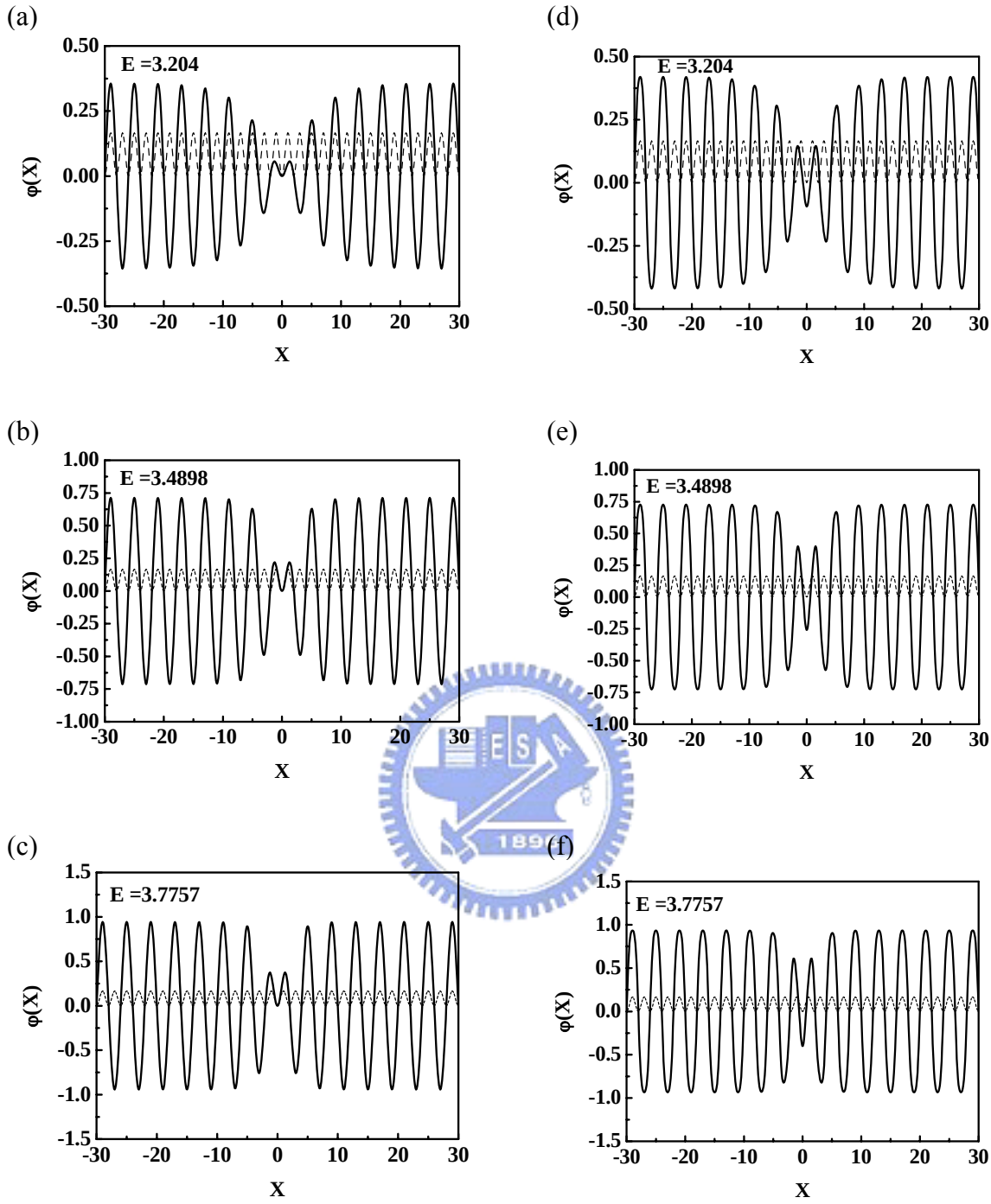

Fig. 7 *b*-type dark soliton for analytic result of $\varphi_b(X) = A\tanh(BX)\frac{1}{\sqrt{\pi}}\sin\left(\frac{\pi X}{2}\right)$ with energy (a) $E = 3.204$, (b) $E = 3.4898$, and (c) $E = 3.7757$ and for the numerical result of G-P equation (d), (e), and (f). The dashed line represents optical lattices.

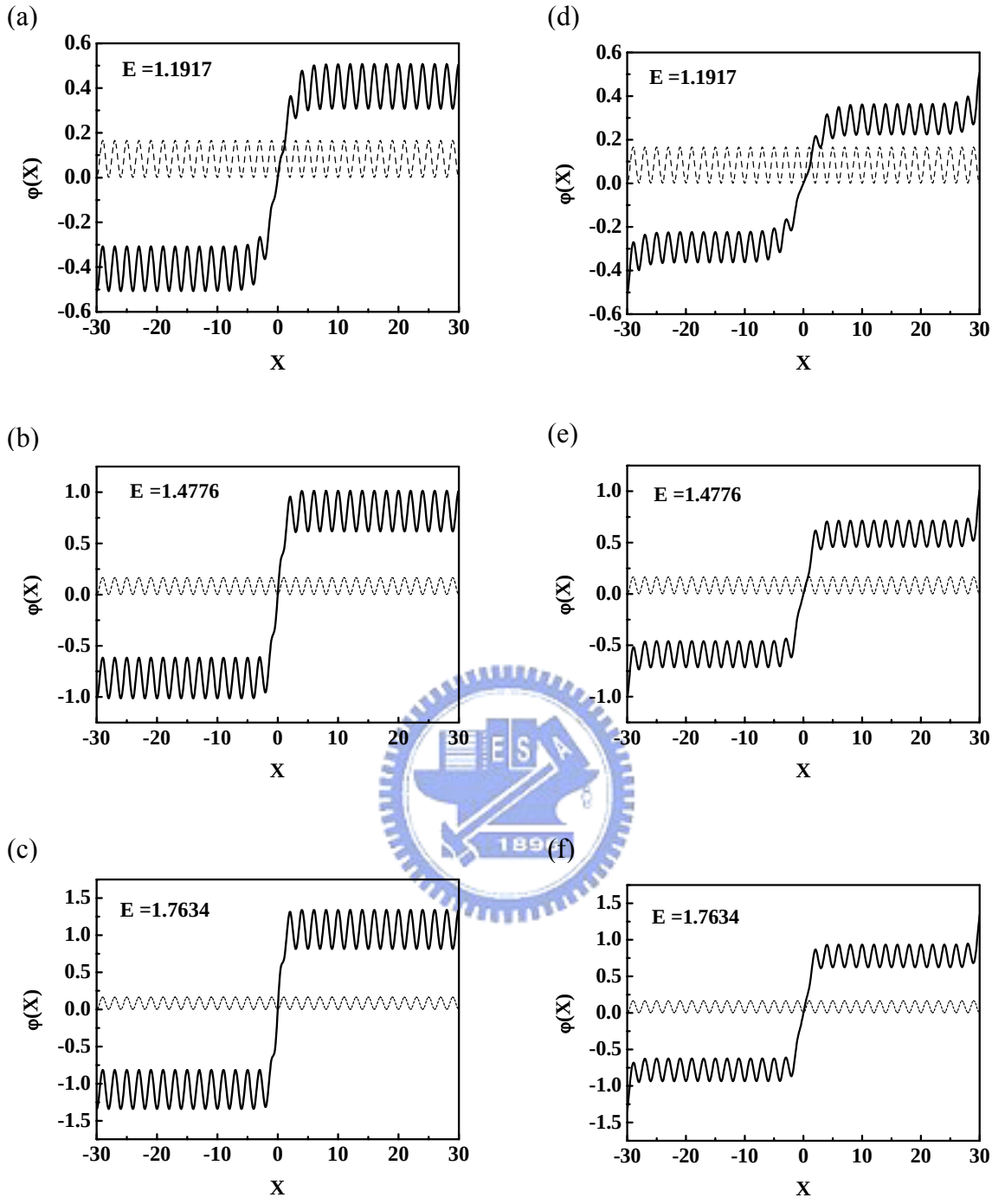

Fig. 8 *c*-type dark soliton for analytic result of $\varphi_c(X) = A\tanh(BX)(b_o + b_{-1}\cos\pi X)$ with energy (a) $E = 1.1917$, (b) $E = 1.4776$, and (c) $E = 1.7634$ and for the numerical result of G-P equation (d), (e), and (f). The dashed line represents optical lattices.

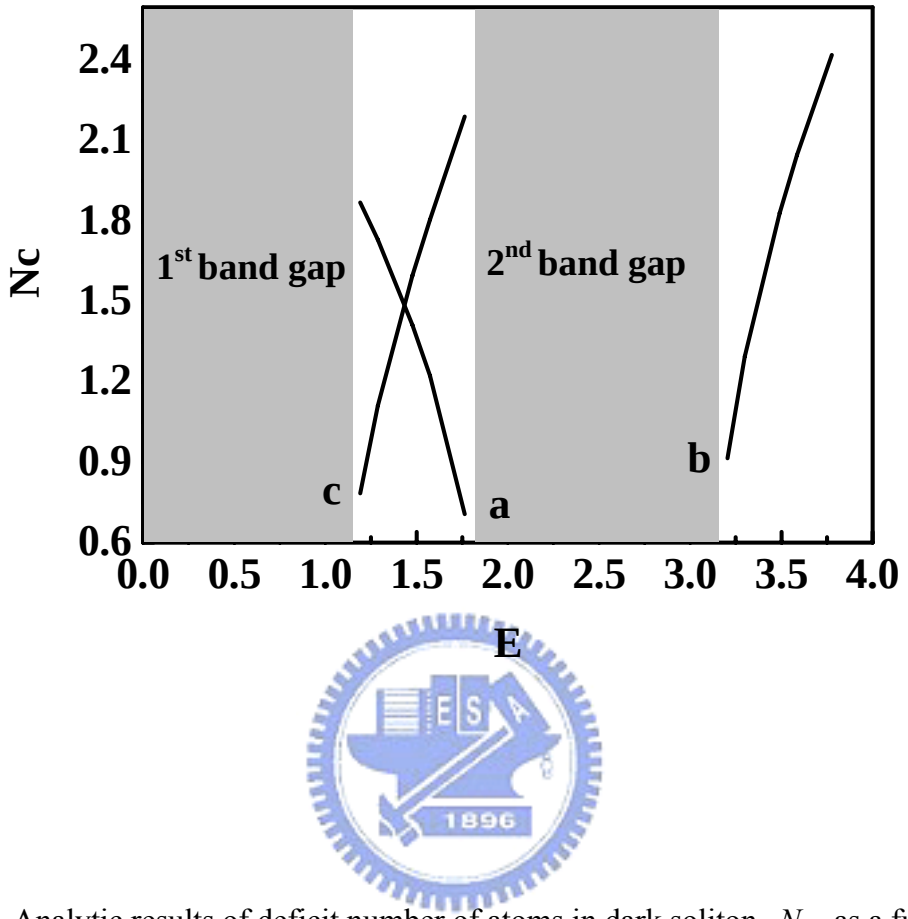

Fig. 9 Analytic results of deficit number of atoms in dark soliton N_c as a function of energy E for a-type, b-type and c-type. The shaded regions are the first and second band gap, respectively.

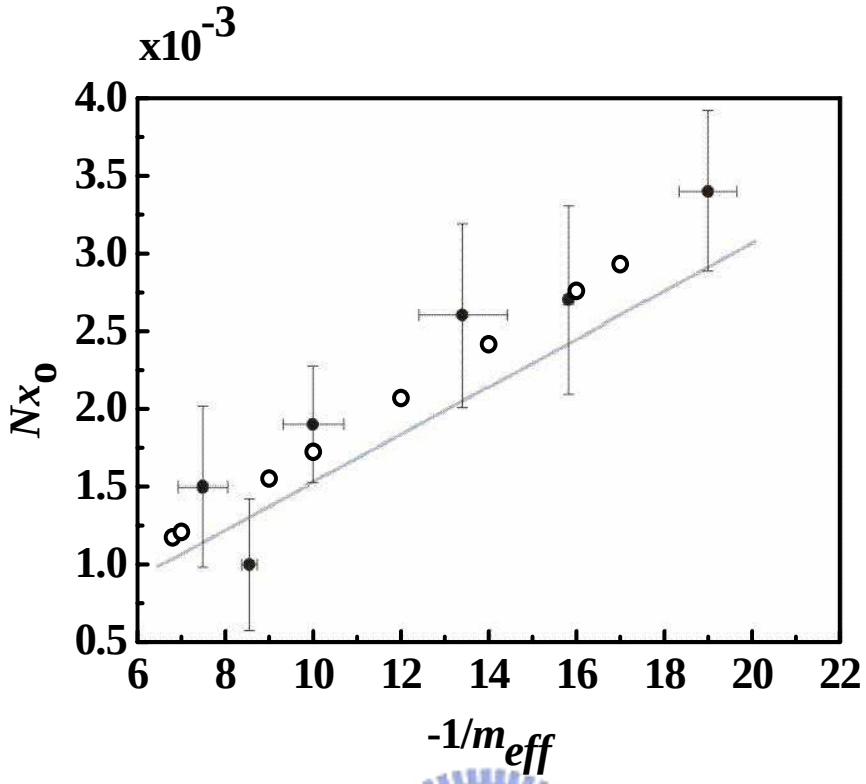

Fig. 10 Product of number of atoms in a-type bright soliton $\boldsymbol{N}$ and soliton width x_o as a function of inverse effective mass $1/m_{eff}$. Comparison of Eiermann *et al.* experimental results (solid circles) and our analytic results (open circles) for the depth of optical lattices V_o is 0.8972.

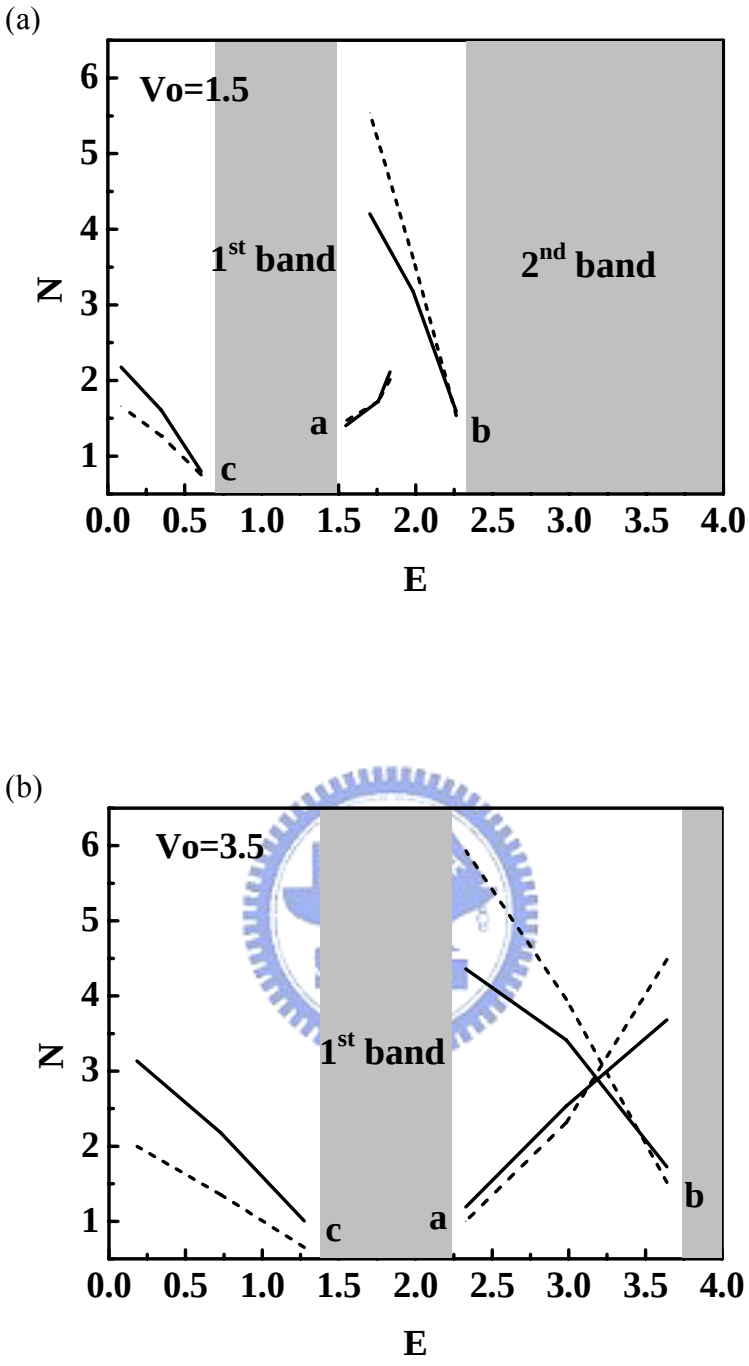

Fig. 11 Number of atoms N and energy E for different depth of optical lattices V_o (a) $V_o = 1.5$ and (b) $V_o = 3.5$. The solid and dashed curves are the analytic and numerical results, respectively.